www.sciencemag.org/cgi/content/full/science.aar2038/DC1

Supplementary Material for

Evidence for hormonal control of heart regenerative capacity during endothermy acquisition

Kentaro Hirose, Alexander Y. Payumo, Stephen Cutie, Alison Hoang, Hao Zhang, Romain Guyot, Dominic Lunn, Rachel B. Bigley, Hongyao Yu, Jiajia Wang, Megan Smith, Ellen Gillett, Sandra E. Muroy, Tobias Schmid, Emily Wilson, Kenneth A. Field, DeeAnn M. Reeder, Malcom Maden, Michael M. Yartsev, Michael J. Wolfgang, Frank Grützner, Thomas S. Scanlan, Luke I. Szweda, Rochelle Buffenstein, Guang Hu, Frederic Flamant, Jeffrey E. Olgin, Guo N. Huang*

*Corresponding author. Email: guo.huang@ucsf.edu

Published 7 March 2019 as *Science* First Release
DOI: 10.1126/science.aar2038

This PDF file includes:

Other Supplementary Material for this manuscript includes the following:
(available at www.sciencemag.org/content/science.aar2038/DC1)

Tables S1, S6, and S7 as separate Excel files

Materials and Methods

Reagents

Following reagents were used: rabbit anti-PCM1 (H262) (1:200) (Santa Cruz Biotechnology SC-67204), rabbit anti-PCM1 (1:2000) (Sigma HPA023370), Rat anti Ki-67 monoclonal antibody (SolA15), eFluor 570 (1:200) (eBioscience 41-5698-80), Mouse anti-Troponin T, cardiac isoform antibody (1:400) (Thermo Fisher Scientific MS295P1), Mouse anti-phospho Histone 3 antibody (1:500) (Millipore Mill-05-806), Rabbit anti-YAP antibody (1:200) (Proteintech, Inc. 13584-1-AP), Rabbit anti-Mef2 (1:75) (Santa Cruz Biotechnology SC-313), Rabbit anti-CPT2 (1:1000) (Millipore ABS85), WGA CF633 conjugates (1:200) (Life Technology 29024), SouthernBiotech Dapi-Fluoromount-G Clear Mounting Media (Southern Biotech 0100-20), 5-Ethynyl-2-deoxyuridine (Santa Cruz Biotechnology SC-284628), Click-it EdU imaging kit (ThermoFisher Scientific C10337), Collagenase Type II (Worthington LS004177), Hydroxypropyl-b-cyclodextrin (Fisher Scientific H0979), NH3 (Thyroid hormone receptor antagonist) (Tom Scanlan lab), Propranolol (Sigma 40543), Cyclosporin A (Sigma PHR1092), GW6471 PPARalpha inhibitor (Sigma G5045), GSK3787 PPARdelta inhibitor (Sigma G7423), T0070907 PPARgamma inhibitor (Sigma T8703), Mifepristone (VWR 89162), Somavert (Ethan Weiss lab), Hydralazine (Spectrum Chemical HO120), Losartan (VWR TCL0232), Atropine (Sigma PHR1379), Nifedipine (Fisher ICN15174301), Iodine deficient diet, 0.15% PTU (Harlan Lab TD.95125), Ethyl carbamate (Alfa Aesar AAA44804-18), ethyl-3-aminobenzoate (Tricaine) (Acros Organics 118000100).

Animals

Mice and zebrafish procedures were conducted in accordance with the Institutional Animal Care and Use Committee (IACUC) of the University of California, San Francisco under animal protocol AN165476-01E. CD-1 (Charles River), *Myh6-Cre* (*29*), *ACTB-Cre* (*30*), *Myh6-*

merCremer (*31*), *TRα*$^{AMI/AMI}$ (named as *Thra*$^{DN/DN}$) (*22*) and *Cpt2*$^{fl/fl}$ (*32*) mouse lines were maintained according to the University of California, San Francisco institutional guidelines. Adult mice were 6-13 weeks old. Ischemia-reperfusion injury experiments were performed in adult male mice (C57BL/6; CD-1 mixed background). For all other experiments, both male and female animals were used and no gender difference was observed. For analysis of cardiomyocyte nucleation and proliferation in wild type mice, CD-1 mice were harvested at P14. Adult zebrafish heart amputation experiments were performed in zebrafish 6 months to 12 months in age. The source of heart tissues of different vertebrate species is listed in Table S2. The hearts were collected from adult animals that died in the laboratory or natural environment. Their ages at the time of death and harvest were estimated based on the record of their body size and weight, and this information confirmed that they had reached sexual maturity and were adults. Based on literature, African clawed frogs are tetraploid and all other species are diploid.

Methods

Generation of mouse lines

Mice heterozygous for the *Tg(Myh6-cre)2182Mds* transgene (hereinafter referred to as "*Myh6-cre*") and *Myh6-merCremer* were crossed with mice homozygous for the *Thra*^{DN} allele to generate *Myh6-cre;Thra*$^{DN/+}$, *Myh6-merCremer;Thra*$^{DN/+}$ and Cre-negative control mice. Similarly, mice heterozygous for the *Tg(ACTB-cre)2MRT* transgene ("*ACTB-cre*") were bred with mice homozygous for the *Thra*^{DN} allele to generate *ACTB-cre;Thra*$^{DN/+}$ and cre-negative littermate controls. *ThraTAG* mice were generated (Guyot, R. and Flamant, F. Manuscript in preparation) by knocking in the TRα locus a sequence encoding TRα1 fused with protein G and Strepavidin binding protein (GS) after a floxed stop cassette. In the presence of Cre, recombination at the loxP sites excises the stop cassette, thus activation expression of GS-TRα1.

Analysis of cardiomyocyte nucleation and ploidy from various species

Ventricular tissues were fixed in 4% paraformaldehyde or formalin for at least two days followed by incubation in 50% w/v potassium hydroxide solution overnight. After a brief wash with PBS, tissues were gently crushed to release dissociated cardiomyocytes. Cells were further washed with PBS three times, deposited on slides, and then allowed to dry out completely. Nuclei were stained with 4',6-diamidino-2-phenylindole (DAPI). To determine cardiomyocyte nucleation, images of spotted cardiomyocytes were analyzed in Photoshop. The number of mono-nucleated, bi-nucleated, and poly-nucleated cardiomyocytes was determined manually using the Count Tool. At least 200 cardiomyocytes per each sample were analyzed.

The ploidy of cardiomyocyte nuclei was determined by normalizing DAPI intensity of cardiomyocyte nuclei to that of non-cardiomyocyte nuclei in the same field. Non-cardiomyocytes are assumed diploid (2N). In details, to demarcate nuclear boundaries, images of the DAPI signal were processed in ImageJ using the following pipeline: Edit → Invert, Image → Adjust → Threshold, Process → Binary → Watershed. After nuclear boundaries were identified, the integrated pixel density of individual nuclei in cardiomyocytes and non-cardiomyocytes were measured manually. All raw integrated pixel density values per each nuclei were organized in an excel spreadsheet. Cardiomyocyte nuclei values were normalized against the average value observed in non-cardiomyocyte nuclei in the same imaging field. Normalized readings were then organized into histograms. The following categorizations were used: 2N cardiomyocyte nuclei were classified as nuclei with normalized integrated pixel densities from 0.5 to 1.5, 4N cardiomyocyte were between 1.5 and 2.5, and nuclei above 2.5 were considered 4N+. See Fig. S2 for an example. At least 200 cardiomyocytes per each sample were analyzed.

Phylogenetically controlled regression analysis

To account for non-independence in traits across closely-related species with a recent common ancestor, we used the method of phylogenetic generalized least squares (PGLS) to create a regression (*33*). This method is comparable to a weighted regression that de-emphasizes data points involving closely related species with a recent common ancestor (*33*). Our phylogenetic tree was constructed using phyloT, a phylogenetic tree generator that uses molecular data from based on NCBI taxonomy, with the polytomy option turned on.

We used the regression equation:

$$Y = b_0 + b_1 X + \varepsilon$$

where b_0 is the y-intercept value of the regression equation, b_1 is the slope of the regression equation, and ε is the residual error which in our case is set to zero.

b_0 and b_1 is calculated using the following equation:

$$\beta = \begin{matrix} b_0 \\ b_1 \end{matrix} = (X'C^{-1}X)^{-1}X'C^{-1}y$$

where *X, X', C*$^{-1}$*,* and *y* are all matrices. *X* and *X'* are the x-value matrices, respectively. *C*$^{-1}$ is the inverse matrix of a matrix as determined by distances of most recent common ancestors on a phylogenetic tree. *y* is the y-value matrix.

The correlation coefficients (R^2) for this PGLS analysis were not shown in Fig. S3 because an official method to calculate a true R^2 value for PGLS regression does not exist (*33*). But we presented the correlation coefficients for all non-phylogenetically controlled regression analyses in Fig. 2.

Drug treatment in the neonatal mice

Chemical administration was performed in CD1 mice. We investigated various neurohormonal, hemodynamic and metabolic pathways that exhibit dramatic changes during the perinatal window such as endocrine systems (thyroid hormone, glucocorticoid hormone, growth hormone), neural activity (sympathetic and parasympathetic activation), renin-angiotensin

activation, blood pressure changes, cardiomyocyte metabolism and hypertrophic responses. The following compounds were administered by a single daily subcutaneous injection from postnatal day 1 (P1) to P14: NH3, propranolol, cyclosporin A, PPARi, mifepristone, somavert, hydralazine, losartan, atropine, and nifedipine. Dosage and preparation information is detailed in Table S5. Propylthiouracil (PTU) was administered by feeding chow containing 0.15% PTU fed to animals at the desired developmental stages. All hearts were harvested at P14 and analyzed for cardiomyocyte nucleation and proliferation as described below.

Cardiomyocyte isolation by collagenase digestion

Isolated cardiomyocytes from freshly harvested hearts were obtained using the Langendorff method. Mice were injected with 6.67 mg/kg bodyweight of heparin (1000 IU/mL) intraperitoneally 30 minutes before anesthetizing the mice with 20% ethyl-carbamate. The hearts were rapidly excised and the aorta was cannulated onto a Langendorff apparatus and perfused with 2 mg/mL collagenase II (Worthington). Digestion was stopped after the hearts lost partial integrity. Hearts were then unmounted from the Langendorff apparatus, ventricles isolated, and gently triturated with forceps to further release cardiomyocytes. Isolated cardiomyocytes were then fixed in 2% PFA for 15 minutes at room temperature, spotted onto glass slides, and stained with DAPI to visualize nuclei.

Immunohistochemistry on mouse tissues

At the desired stages, mice were anesthetized by injection of 20% ethyl carbamate in 1X PBS, their hearts were freshly excised, soaked briefly in 30% sucrose, and then embedded in O.C.T. Compound (Tissue Tek, cat#4583) and flash frozen on a metal block cooled by liquid nitrogen. Embedded samples were then sectioned with a Leica CM3050S to 5 μm thickness. Tissue sections were then fixed in 3.7% formaldehyde for 15 min at room temperature, permeabilized in 0.2% Triton X-100 in PBS (PBST), blocked in 5% normal donkey serum (NDS)

in PBST for 1 hour at room temperature, and incubated with primary antibodies in PBST overnight at 4°C. After primary antibody incubation, sections were incubated in their corresponding secondary antibody (Alex Fluor 488, 55, 647; Invitrogen, 1:500) for 2 hours at room temperature. In experiments labeling the cell membrane, incubation with wheat germ agglutinin (Biotin, 1:200) was performed alongside secondary antibody incubation. In all samples, nuclei were visualized by staining with DAPI.

Quantification of total cardiomyocyte number

For collagenase dissociation analyses, hearts were fixed in 3.7% formaldehyde for 1 hour. After removal of the atria, the ventricle was then cut into four pieces and digested in PBS containing 2 mg/ml collagenase II (Worthington) with gentle shaking at 37°C until complete digestion (~1 week). The digestion buffer was changed daily. All dissociated cardiomyocytes were pooled and counted using a hemocytometer.

For stereological analysis, estimation of total cardiomyocyte number was performed as previously described (20). Briefly, heart ventricles were cut into small pieces (1-2 µm diameter). Heart pieces were picked randomly, and then embedded into an 8% gelatin isector with 3 mm diameter. The isectors were embedded in O.C.T Compound, and 40 µm-thick cryosection were stained with cardiomyocyte marker, PCM1. A minimum of 3-4 isectors were analyzed, and a minimum of 200 cardiomyocytes were quantified per animal. To estimate total cardiomyocyte nuclei numbers, images were acquired on a Nikon Eclipse Ti Spinning Disk, and analyzed with FIJI (Fiji is Just ImageJ) software. A systematic random sampling scheme (meander samping) was applied with a counting frame (40 µm x 40 µm x 20 µm, and 3 µm guard zones for P14 hearts and 70 µm x 70 µm x 20 µm, and 3 µm guard zones for adult hearts). Total cardiomyocyte number was calculated based on ventricle weight and cardiomyocyte nucleation data.

Quantification of cardiomyocyte volume

Fixed cardiomyocytes isolated from P14 and adult mice were placed on a slide glass, and then imaged using a Leica TCS SPE confocal microscope by obtaining optical sections (1.5 μm axial interval). The analysis was performed using Imaris software to obtain a cell volume for each cardiomyocytes. A minimum of 200 cardiomyocytes per animal was quantified.

RNA-seq analysis

RNA was isolated from P14 ventricle samples using TRIzol Reagent (Thermo Fisher Scientific) according to a manufacturer's instruction and further pre-cleaned by Zymo RNA Clean & Concentrator. 1 μg total RNA was used for RNA-seq library preparation. mRNA was enriched, fragmented, first and second-strand synthesized using the Illumina Tru-seq RNA Library Prep Kit V2. mRNAs were then subjected to end-repaired, A-tailing, adaptor ligation and PCR amplification using the NEXTflex Rapid DNA-Seq kit.

RNA-seq reads with quality less than 20 were removed after trimming adapter with cutadapt(v1.9). Reads were mapped to the mm10 reference with STAR(v2.5.2b) with parameters of --outFilterMismatchNoverLmax 0.04. Gene count matrix was generated with featureCounts(v1.5.1). Differential expressed genes were calculated and selected with DESeq2 fold change 1.5 and adjusted p-value 0.05. This dataset is summarized in Table S6 and has been deposited in Gene Expression Omnibus (GEO) under accession number GSE125596.

ChIP-seq analysis

Heart chromatin was prepared from P14 *Myh6-Cre;TAG-TRα1* mice expressing GS-TRα1 in cardiomyocytes. The protein G tag was used for IgG immunoprecipitation and the DNA fraction was sequenced on an Ion Proton sequencer. The input fraction was used as negative control. We obtained 37 millions reads for the control and 42 millions for a pool of 3 libraries

from different mice. The fastq files were converted to bam file using bowtie2 (all on a local Galaxy platform) after aligning with the mouse genome mm10 (Grc38/mm10). The ChIP-seq peaks with reads more than 35 were considered positive. This dataset has been deposited in Gene Expression Omnibus (GEO) under accession number GSE125414.

Reactive oxygen species measurement

Freshly cut 5 μm heart sections were incubated in 10 μM Dihydrorhodamine 123 (Life Technologies, D-23806) in PBS for 30 min in the dark at 37℃. Sections were then washed with PBS and then stained with DAPI to visualize nuclei. Relative ROS signal intensities were measured using ImageJ.

Mouse EdU analysis

For analysis at P14, animals were injected with 50 mg/kg EdU (reconstituted in saline) intraperitoneally at P12 and P13, followed by heart isolation at P14. For adult mice, animals were injected with 50 mg/kg EdU (reconstituted in saline) intraperitoneally once daily for 10 days (days 1-10 post surgery), and then sacrificed at 28 days post-surgery. Mouse cardiomyocytes were isolated from freshly harvested hearts using the Langendorff method. EdU incorporated cardiomyocytes were visualized via conjugation of sulfo-Cyanine 5-azide dye (Lumiprobe, A3330). All nuclei were stained with DAPI. Nucleation of EdU-positive cardiomyocytes were manually counted, and the the ploidy of EdU-positive cardiomyocyte nuclei was determined by normalizing DAPI intensity of cardiomyocyte nuclei to that of non-cardiomyocyte nuclei in the same field (as described above).

Mitochondrial DNA quantification

DNA was purified from frozen P14 heart ventricles with Proteinase K, following by phenol/chloroform extraction. qPCR was performed using the SYBR Select Master Mix (Applied Biosystems, 4472908) and the 7900HT Fast Real-Time PCR system (Applied Biosystems). Mitochondrial DNA content was measured via qPCR targeting mitochondrial genes, *ND2* and *Cox1*, and Relative mitochondrial DNA content was measured with qPCR targeting mitochondrial genes, *ND2* and *Cox2*, and normalization against genomic gene, *H19* using the following primers: *mtND2* forward=5'- CCCATTCCACTTCTGATTACC-3'; *mtND2* reverse= 5'-ATGATAGTAGAGTTGAGTAGCG-3'; *mtCox1* forward =5'- CTGAGCGGGAATAGTGGGTA-3'; *mtCox1* reverse= 5'- TGGGGCTCCGATTATTAGTG-3'; *H19* forward =5'-GTCCACGAGACCAATGACTG-3' ; *H19* reverse =5'-GTACCCACCTGTCGTCC-3'.

GSH and GSSG measurement

Quantification of GSH and GSSG was described in a previous paper (*34*). GSH and GSSG were extracted from frozen P14 mouse heart ventricles.

Ischemia reperfusion

Ischemia reperfusion injury was induced in *Myh6-cre; Thra*$^{DN/+}$ and *Thra*$^{DN/+}$ littermate controls by ligation of the LAD for 45 min and then releasing the suture as previously described (*35*). The surgeon was blind to the animal genotype. In short, male mice 6 to 12 weeks old were anesthetized using an induction dose of 5.0% isofluorane mixed with oxygen. Endotracheal intubation was performed and the animal was maintained on a ventilator with 1.0% isofluorane throughout the duration of the surgery. After thoracotomy, the LAD was ligated for 45 min, released, and chest wall and skin were closed. The animals were extubated and allowed to recover.

Echocardiography

Left ventricular systolic function was evaluated by two-dimensional echocardiography with Visual Sonics Vevo 3100 equipped with a 40 MHz probe. Animals were anesthetized with 0.5-1.0% isofluorane and hair was removed over the measurement area. The mice were then placed in a supine position on a heating pad. To measure ejection fraction and fractional shortening, short axis images were acquired at the level of the papillary muscle with M-mode, and the left ventricle internal dimensions (LVIDs) were determined in both diastole and systole.

Histology

Freshly dissected or formaldehyde fixed hearts were cryo or paraffin embedded, respectively. For fibrosis analysis, either 5 μm cryosections or 5 μm paraffin sections were fixed in Bouin's fixative overnight at 55°C, and stained with Fast Green FCF for 30 min and Sirius Red for 25 min at room temperature. For eosin and hematoxylin staining, 5 μm paraffin sections were stained with Eosin for 3 min and hematoxylin for 5min at room temperature. Sections were imaged using Axio Scan.Z1 and fibrotic area was quantified using ImageJ.

Blood pressure measurement

Blood pressure in P14 mice was evaluated by two-dimensional echocardiography with Visual Sonics Vevo 3100 equipped with a 40 MHz probe. Blood pressure was measured in animals without anesthesia by restraining the animals by hand. Short axis images of heart were acquired with M-mode. Heart rate was automatically calculated during echocardiography analysis.

Body temperature measurement

For mouse, rectal temperature was measured using THM150 (Visualsonics). For zebrafish, body temperature was acquired using an infrared red camera, FLIR-E64501 (FLIR).

Western blotting

For western blotting analysis, proteins were lysed in 1% SDS (reconstituted in PBS) supplemented proteinase inhibitor (Fisher, PI88666) from frozen P14 mouse heart ventricles. Protein concentration was measured using the BCA Protein Assay Kit (Pierce). 100mg protein lysate was first loaded to a NuPAGE 4-12% Bis-Tris Gel (Invitrogen) for separation, and then transferred to a PVDF membrane (BIO-RAD). Protein loading was assessed using Ponceau S staining. The blot is visualized using ECL Western Blotting substrate (Pierce).

Zebrafish regeneration study

Ventricular resections on *Danio rerio* (EKW background) aged 1-2 years were performed as described (*5*). Fish were lightly sedated using Tricaine and placed the ventral-side up in a damp slotted sponge to keep the gills moist. The beating heart could be visualised under the upper abdomen. The scales were removed around this area using fine forceps and a small incision was made directly at the location of the heart. By applying gentle pressure to the body, the apex of the heart was squeezed out of the incision and the apex cut off using iridectomy scissors. This was followed by a roughly 60 second period of bleeding from the wound whist allowing a clot to form to seal the wound. Approximately 2 minutes after apical resection the fish was returned to water and encouraged to recover from Tricaine sedation by pipetting water over the gills.

For T3 treatment, fish were placed in 2L static tanks with 5 nM T3 at a density of no greater than 7 fish/2L. Water was changed daily for the first two weeks and then once in two days thereafter to minimize stress on the fish. EdU injections were performed by lightly sedating the fish using Tricaine and injecting 100 µl of 2 mM EdU into the lower abdomen. Fish hearts were harvested for fixation by killing the fish in tricaine solution and then making a large incision in the abdomen above the heart. The heart was then removed from the body cavity, taking care to preserve the structures of the outflow tract, atrium and ventricle. The heart was then fixed in

3.7% formaldehyde for 1 hour, equilibrated in 30% (w/v) sucrose/PBS, embedded in O.C.T. Compound and snap frozen using liquid nitrogen.

To analyse EdU incorporation into proliferating CMs, 5µm sections were taken of the heart before performing antigen retrieval to reveal Mef2 antigens that mark CMs. Antigen retrieval was achieved by boiling the slides in 10 mM sodium citrate buffer pH 6.0 (0.05% Tween) at 90°c for 30 mins and allowing the slides to cool to room temperature. The sections were then blocked with 5% normal donkey serum for one hour before staining with Mef2 primary antibody over-night at 4°c followed by secondary antibody for 2 hours at room temperature. EdU incorporation was labelled with sulfo-Cyanine 5-azide dye. All nuclei stained using DAPI mounting media. Hearts were imaged using a Nikon Eclipse Ti microscope with Nikon DS-Qi2 camera. The percentage of EdU incorporated CMs was quantified at the border zone within the area 100 µm from injury site using ImageJ and Photoshop software.

Methods for cardiomyocyte isolation from zebrafish ventricles and ploidy assessment were described previously (*4*). Briefly, dissected fish ventricles were incubated in a solution of 0.2% trypsin, 0.8 mM EDTA (Gibco, 25200-056) supplemented with 20 mM glucose and 10 mM 2,3-butanedione monoxime (BDM) for 30 min on ice and then in a solution of Accumax (EMD Millipore, SCR006) supplemented with 20 mM glucose and 10 mM BDM for 45 min at room temperature. Hearts were dissociated into cardiomyocytes by gentle pipetting. Isolated cardiomyocytes were fixed in 4% formaldehyde in PBS. All nuclei were then visualized with DAPI mounting media. Details of cardiomyocyte nucleation and ploidy measurement were explained above.

Heart fibrosis was determined by acid fuchsin orange G (AFOG) staining 30 days post-apical resection. Briefly, fish were euthanized and hearts were harvested while keeping the atrium and outflow tract intact. The hearts were rinsed heart in chilled PBS; and all hearts were kept in chilled PBS until every fish had been harvested. Hearts were fixed in 4% PFA for 1 hour at room temperature and after a brief rinse with PBS, equilibrated in 30% sucrose on ice for 1

hour and embedded in O.C.T. compound. Hearts were snap-frozen with liquid nitrogen. Each heart was sectioned in 10 μm slices. Sections were then fixed with 4% PFA for 15min and washed in 0.5% PBST for 10 min. Slides were transferred into preheated Bouins fixative for 2.5 hr at 56°C and one more hour at room temperature. Slides were then washed in tap water twice for 20 minutes, incubated in 1% phosphomolybdic acid for 5 minutes, and rinsed with distilled water, incubated in AFOG staining solution 5 minutes, and washed twice in distilled water. Finally, the samples were dehydrated in 95% EtOH for 5 min, twice in 100% EtOH for 2min, cleared in xylene for 2 min, and mounted in Fluormount.

Zebrafish fin regeneration

Caudal fin amputation was performed as described previously (*36*). Zebrafish were anesthetized with tricaine and their caudal fins were amputated with a razor blade. For T3 treatments, fish were placed in 2L static tanks with 5 nM T3. Fish water was replaced daily. Fin regeneration was observed at 14 days post amputation.

Serum T3 and T4 measurements

Blood was harvested from the aortic vessel of adult zebrafish and facial vein of neonatal mice. Serum was collected after the blood was allowed to clot. Total T4 and T3 concentrations were determined using commercial ELISA kits (Abnova cat#KA0200; Invitrogen cat#EIAT3C)".

Neonatal mouse cardiomyocyte isolation and culture

Freshly dissected ventricles from P2 mice were cut into 4 pieces, and then washed with perfusion buffer (12mM NaCl, 1.5mM KCl, 60μM KH_2PO_4, 60μM Na_2HPO_4, 120μM $MgSO_4$, 1mM HEPES, 4.6mM $NaHCO_3$, 30mM Taurine, 10mM BDM and 5.5mM Glucose). Cardiomyocytes were isolated in digestion buffer (2mg/ml collagenase II in perfusion buffer) for 2h at 37℃ during agitation. Isolated cardiomyocytes were cultured in 10%FBS in DMEM

supplemented penicillin streptomycin. Generating hormone-depleted FBS is described before (*37*). Briefly, Activated charcoal (Sigma #C9157) and Dextran T-70 (Sigma # D8821) were added heat inactivated FBS to final concentrations of 1% and 0.1%, respectively, incubated at room temperature for 1 hour with agitation, centrifuged and filtered to obtain the depleted serum.

Statistical analysis

The number of samples per each experimental condition is listed in the description of the corresponding figure legend. Statistical significance was determined using the Chi-square test (Fig. S20C), one-way ANOVA test followed by Bonferroni corrections (Fig. 4 D and G; Fig. S18C), and Student's T-test for the rest of figures (for values that are expressed in percentages, data were first transformed by conversion to arcsin values before comparison in the Student's T-test). Error bars are represented as standard error of the mean.

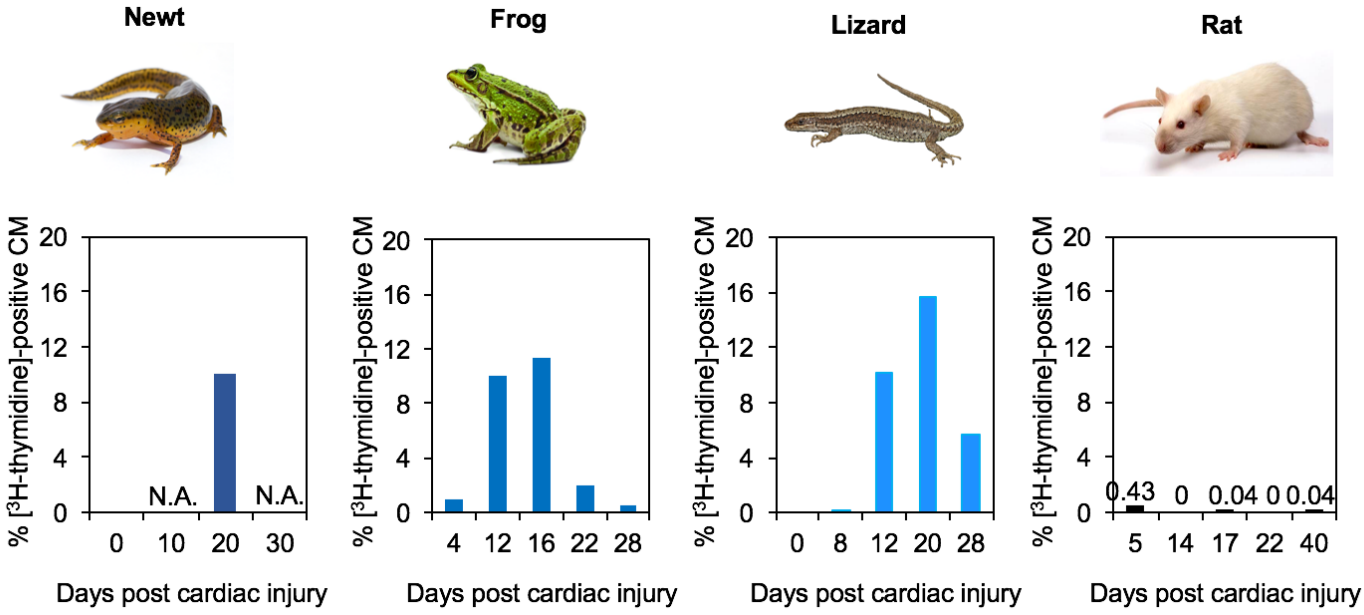

Figure S1. Comparison of cardiomyocyte (CM) proliferation following myocardial injury in adult newts, frogs, lizards and rats. Radiolabelled thymidine was used to label proliferating CMs. This figure is plotted based on previously reported data (*6*, *65*).

A

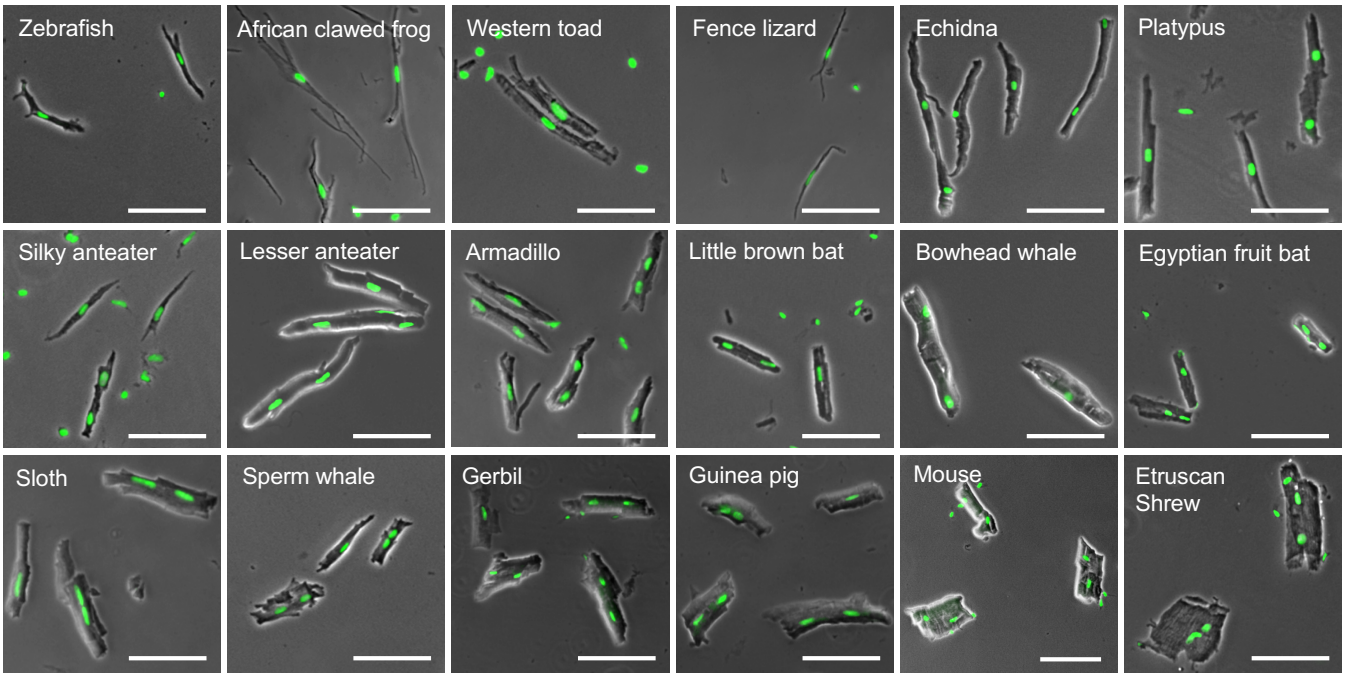

B Dissociated cardiomyocytes from Sperm whale (*Physeter macrocephalus*)

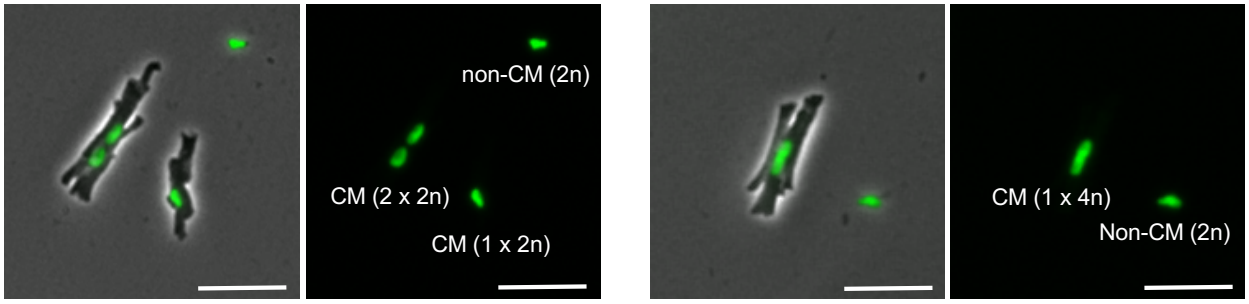

C

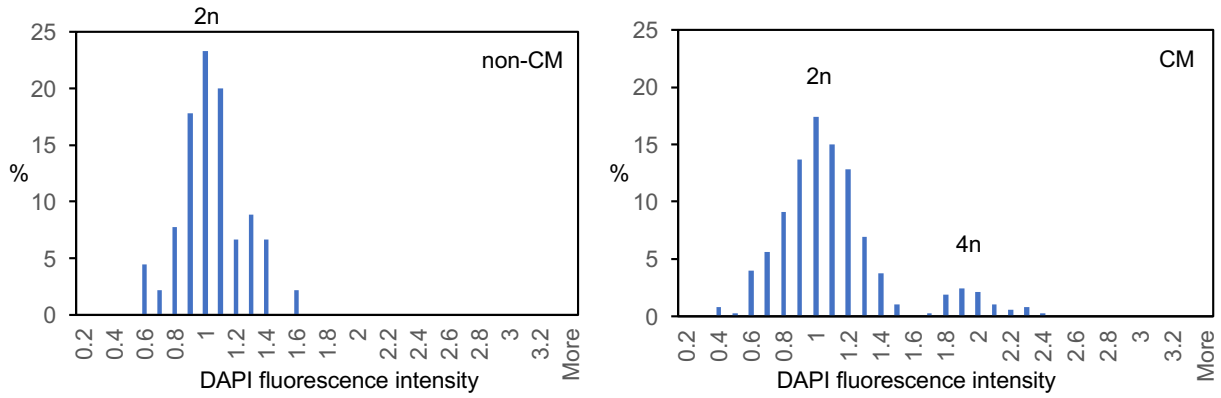

D

	Diploid	Tetraploid		Multiploid			
	1 x 2n	1 x 4n	2 x 2n	2 x 4n	3 x 2n	4 x 2n	other
Field 1	8	1	18	0	3	1	2
Field 2	7	3	27	0	3	0	2
Field 3	21	4	38	0	1	2	2
Field 4	3	2	20	0	0	2	1
Field 5	6	3	9	4	3	1	4
∑:	45	13	112	4	10	6	11
%:	22.4	6.5	55.7	2	5	3	5.4

Figure S2. Representative images of dissociated cardiomyocytes and ploidy assessment using sperm whale cardiomyocytes (CMs) as an example. (**A**) Representative images of dissociated CMs. Nuclei are stained with DAPI (green). Scale bars, 100 μm. (**B**) Images of dissociated sperm whale CMs. Nuclei are stained with DAPI. Shown are examples of diploid non-cardiomyocytes (non-CMs) (2n), a mononucleated diploid CM (1 x 2n), a binucleated tetraploid CM (2 x 2n), and a mononucleated tetraploid CM (1 x 4n). Scale bars, 50 μm. (**C**) Method of ploidy assessment. The distribution of DAPI fluorescence intensity of all nuclei of non-CMs and CMs in the same field is plotted. All values are normalized to the mean fluorescence intensity of non-CMs. (**D**) Example of nucleation and ploidy analysis of sperm whale CMs (>200 CMs from five image fields).

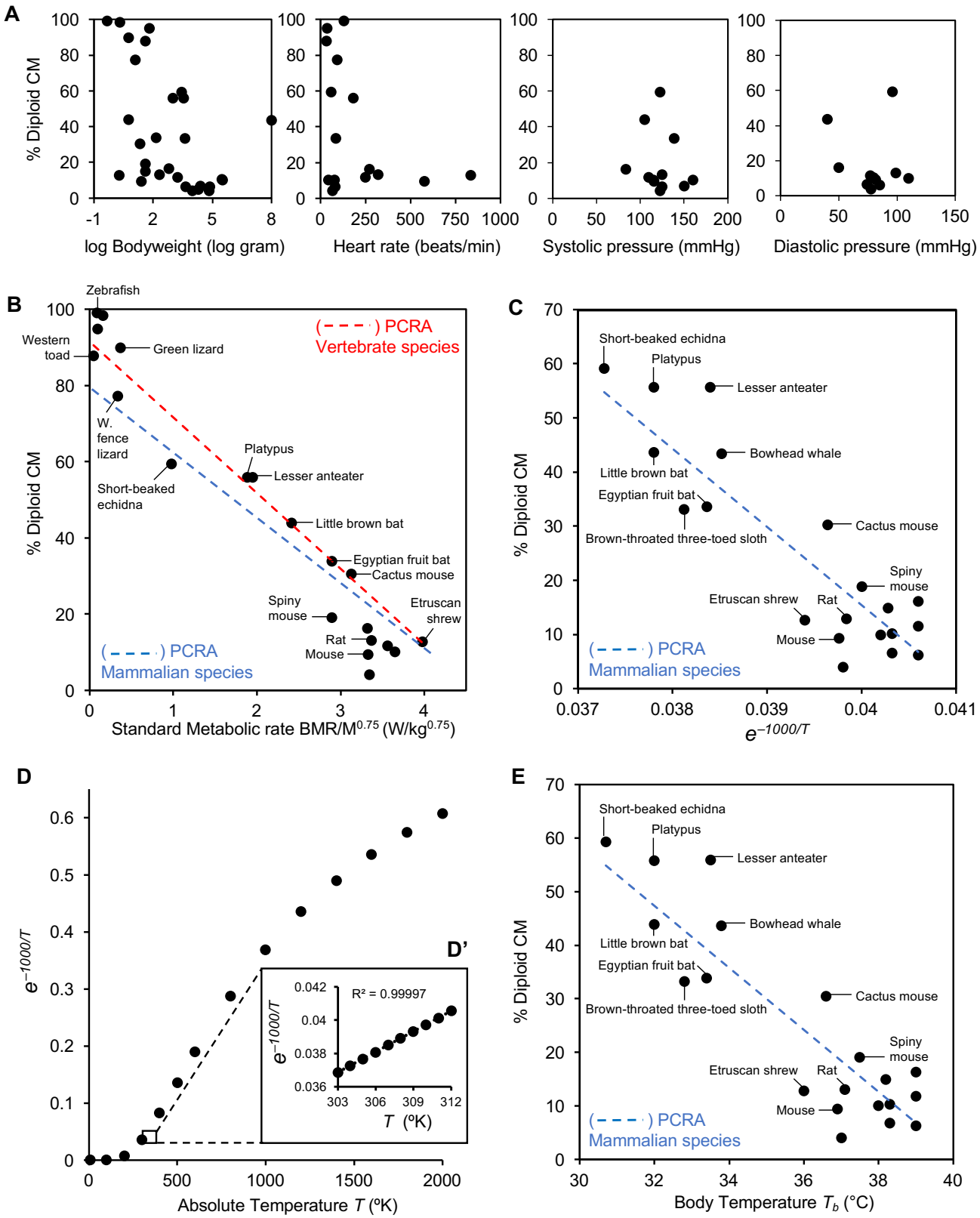
A
% Diploid CM
log Bodyweight (log gram)
Heart rate (beats/min)
Systolic pressure (mmHg)
Diastolic pressure (mmHg)
B
Zebrafish
Western toad
Green lizard
W. fence lizard
Short-beaked echidna
Platypus
Lesser anteater
Little brown bat
Egyptian fruit bat
Cactus mouse
Spiny mouse
Etruscan shrew
Rat
Mouse
(- - -) PCRA
Vertebrate species
(- - -) PCRA
Mammalian species
% Diploid CM
Standard Metabolic rate BMR/M0.75 (W/kg0.75)
C
Short-beaked echidna
Platypus
Lesser anteater
Bowhead whale
Little brown bat
Egyptian fruit bat
Brown-throated three-toed sloth
Cactus mouse
Spiny mouse
Etruscan shrew
Rat
Mouse
(- - -) PCRA
Mammalian species
% Diploid CM
e−1000/T
D
D'
e−1000/T
R² = 0.99997
T (ºK)
Absolute Temperature T (ºK)
E
Short-beaked echidna
Platypus
Lesser anteater
Bowhead whale
Little brown bat
Egyptian fruit bat
Brown-throated three-toed sloth
Cactus mouse
Spiny mouse
Etruscan shrew
Rat
Mouse
(- - -) PCRA
Mammalian species
% Diploid CM
Body Temperature Tb (°C)

Figure S3. Relationships between various physiological parameters and the percentage of mononucleated diploid cardiomyocytes (CMs). (**A**) Effects of bodyweight, heart rates and blood pressures on the frequency of mononucleated diploid CMs. (**B**) Effect of standard metabolic rate ($BMR/M^{0.75}$, in $W/kg^{0.75}$) on the content of mononucleated diploid CMs. This plot is generated using reported data of the basal metabolic rate (*BMR*, in W) and mass (*M*, in kg) of individual organisms. The data are fit by regression lines (red for vertebrate species and blue for mammalian species). (**C**) Effect of $e^{-1000/T}$ on the frequency of mononucleated diploid CMs. *T* represents absolute temperature and *e* is Euler's constant. (**D**) Effect of temperature (*T*, in K) on $e^{-1000/T}$. Inset (D') shows the linear relationship in the range of 303-312 K, which corresponds to the range of mammalian body temperature 30-40°C. (**E**) Effect of body temperature (T_b, in °C) on the percentage of mononucleated diploid CMs. In (**B**, **C**, **E**) phylogenetically controlled regression analysis (PCRA) was performed as indicated to control for the phylogenetic autocorrection introduced by shared ancestry.

Animal species	Latin name	% Diploid CM	BMR/BW$^{0.75}$ (W/kg$^{0.75}$)	Body Temperature (℃)	lgBM (lg Gram)
Short-beaked echidna	*Tachyglossus aculeatus*	59.3	1.0	30.7	3.5
Platypus	*Ornithorhynchus anatinus*	55.8	1.9	32.0	3.0
Lesser anteater	*Tamandua tetradactyla*	55.9	2.0	33.5	3.5
Little brown bat	*Myotis lucifugus*	43.8	2.4	32.0	0.8
Egyptian fruit bat	*Rousettus aegyptiacus*	33.8	2.9	33.4	2.2
Rabbit	*Oryctolagus cuniculus*	11.7	3.6	39.0	3.3
Guinea pig	*Cavia porcellus*	16.3	3.3	39.0	2.8
Mouse	*Mus musculus*	9.4	3.3	36.9	1.4
Rat	*Rattus norvegicus*	13.0	3.4	37.1	2.3
Calf	*Bos taurus*	10.0	3.7	38.0	5.5
Spiny mouse	*Acomys cahirinus*	19.0	2.8	37.5	1.6
Cactus mouse	*Peromyscus eremicus*	30.4	3.1	36.6	1.3
Etruscan shrew	*Suncus etruscus*	12.8	4.0	36.0	0.3
Gerbil	*Meriones unguiculatus*	14.9	3.2	38.2	1.6
Gray wolf	*Canis lupus*	6.7	3.3	38.8	4.4
Human	*Homo sapiens*	4.0	3.4	37.0	4.8

Multivariate regression statistics

Multiple R	0.95
R2	0.90
Adjusted R2	0.87
Significance F	3.45×10^{-6}
	P-value
BMR/BM$^{0.75}$	0.0061
Body temperature	0.043
lgBM	0.44

Figure S4. Multivariate regression analysis of % Diploid cardiomyocytes (CM) and other physiological parameters. BMR, basal metabolic rate. BM, body mass. Parameters that show correlation *P*-value less than 0.05 are highlighted in red.

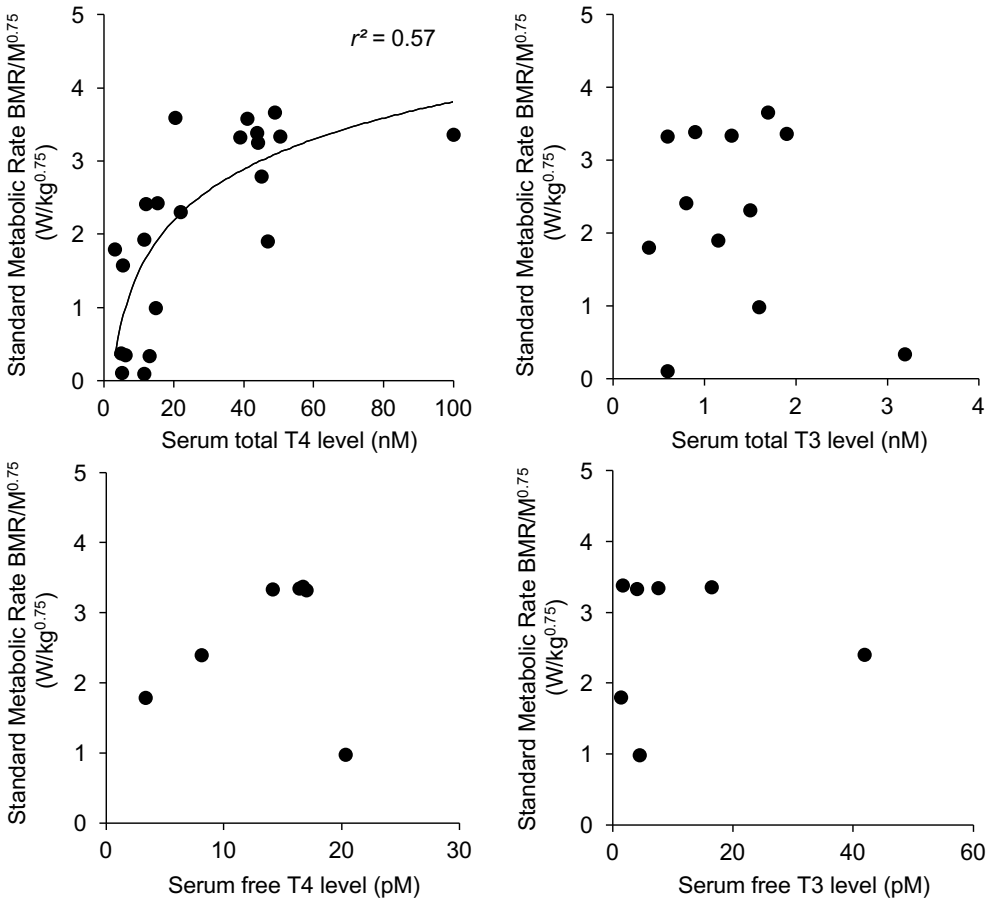

Figure S5. Serum total T4 concentration correlates with Standard Metabolic Rate. These plots include thyroid hormone data from (*11*) and standard metabolic rate data from the Animal Ageing and Longevity Database.

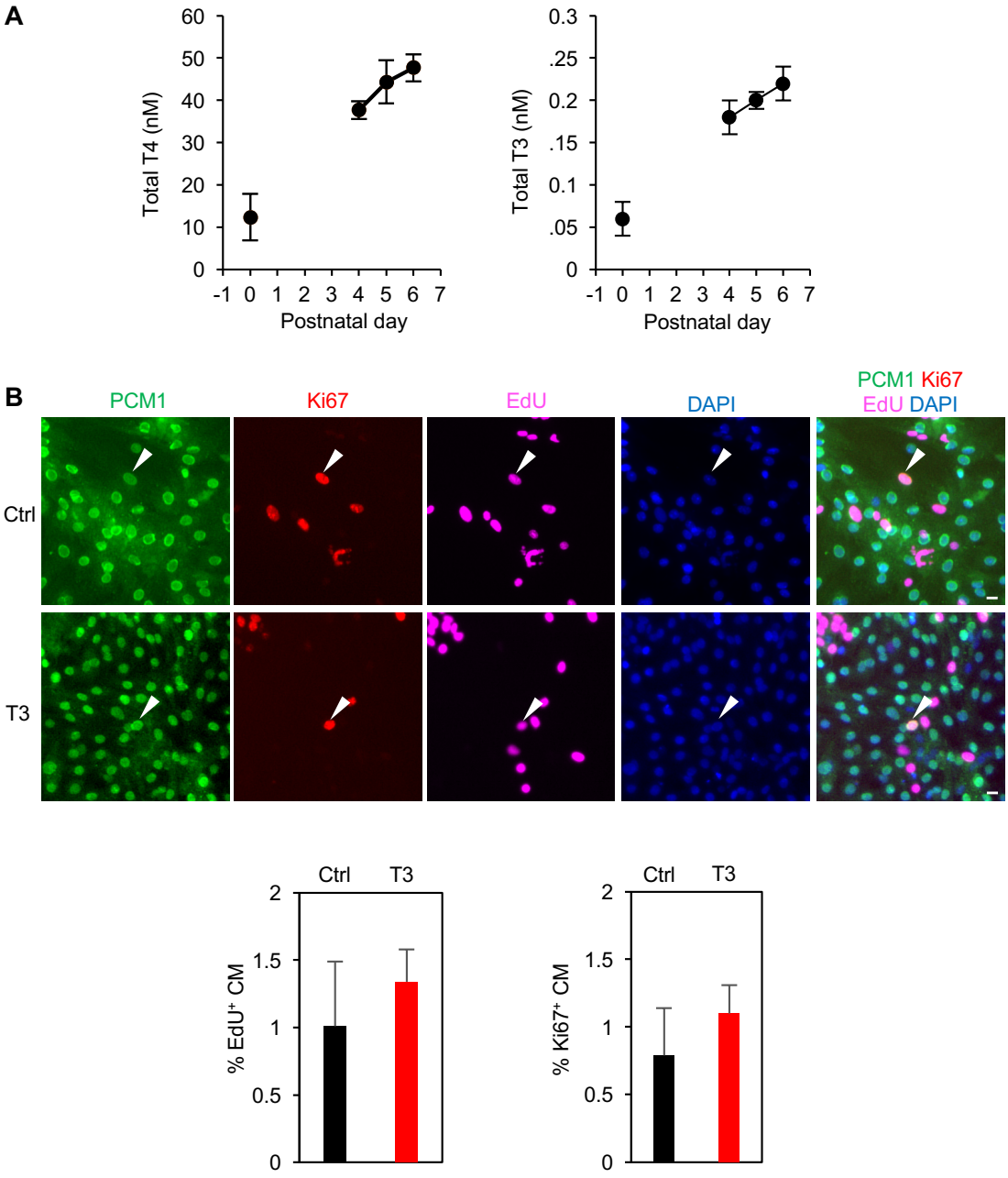

Figure S6. Postnatal thyroid hormone levels and effect of exogenous T3 in regulating cardiomyocyte proliferation *in vitro*. (**A**) Serum total T4 and T3 concentrations at the indicated time points (n=3). (**B**) T3 does not influence neonatal mouse cardiomyocyte proliferation *in vitro*. CM nuclei are stained positive for PCM1. EdU-incorporated or Ki67-positive CMs are examined 72 hours after plating. Quantifications are presented (n=3). Scale bars, 10 μm.

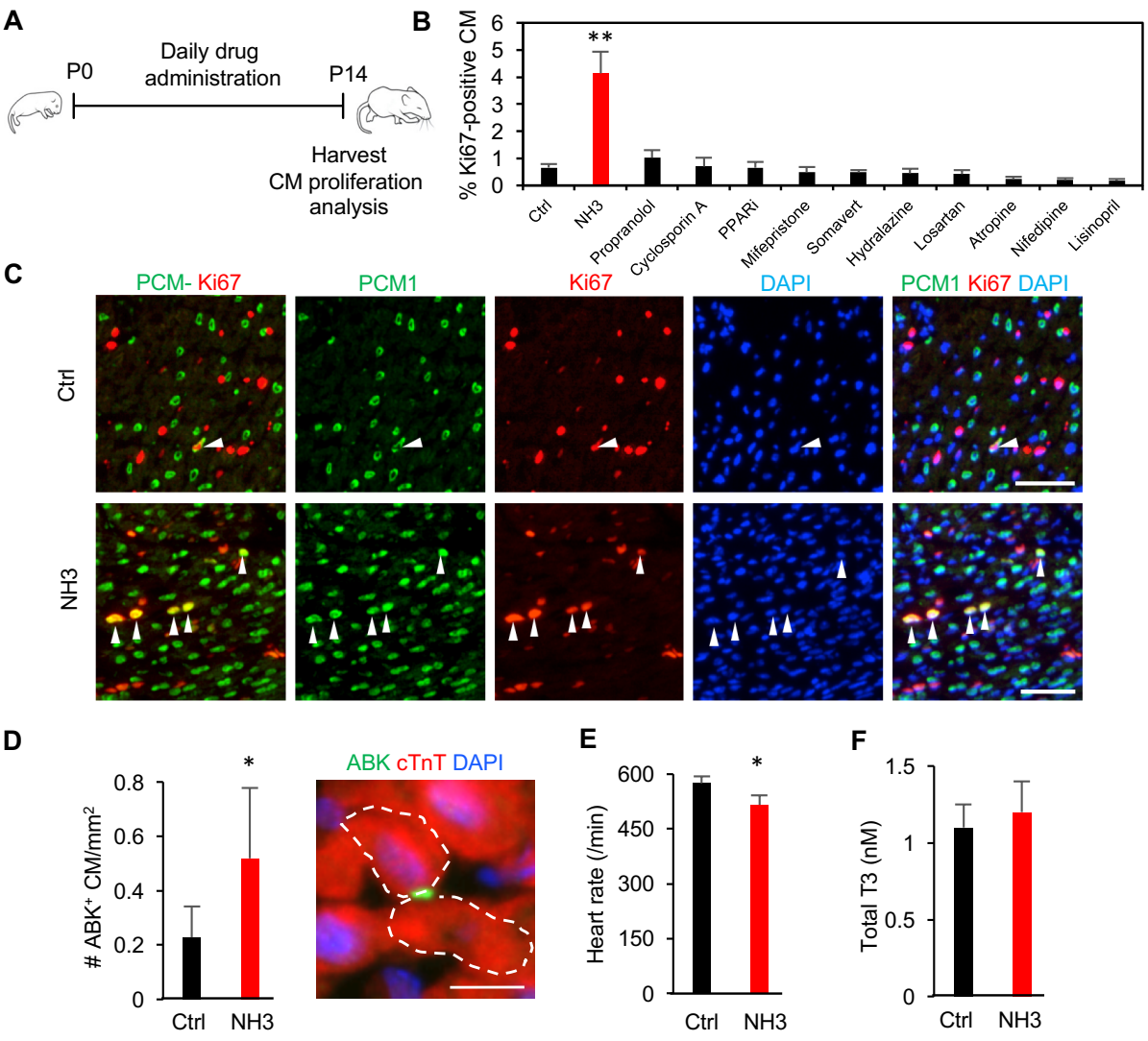

Figure S7. Identification of thyroid hormone receptor activation as a primary trigger of postnatal mammalian cardiomyocyte (CM) cell cycle arrest. (**A**) Schematic of functional pharmacological tests *in vivo* and analysis at postnatal day 14 (P14). (**B**) Quantification of Ki67-positive CM (PCM1 positive) in drug-treated hearts (n=3-6 animals). Chemicals that target neurohormonal, hemodynamic, metabolic pathways that have previously been reported to display drastic activity changes during the perinatal window are chosen. (**C**) Representative images of heart sections from NH3-treated animals. White arrowheads indicate Ki67-positive cardiomyocytes. (**D**) Quantification and representative image of CMs undergoing cytokinesis with Aurora B Kinase (ABK) in the cleavage furrow (n=3 animals). Cardiomyocytes undergoing cytokinesis are outlined. (**E**) Heart rates of control and NH3-treated mice at P14 (n=3 animals). (**F**) Serum total T3 levels in control and NH3-treated mice at P14 (n=3 animals). Values are reported as Mean ± SEM. * P<0.05, ** P<0.01. Scale bars, 100 μm in (**C**) and 20 μm in (**D**).

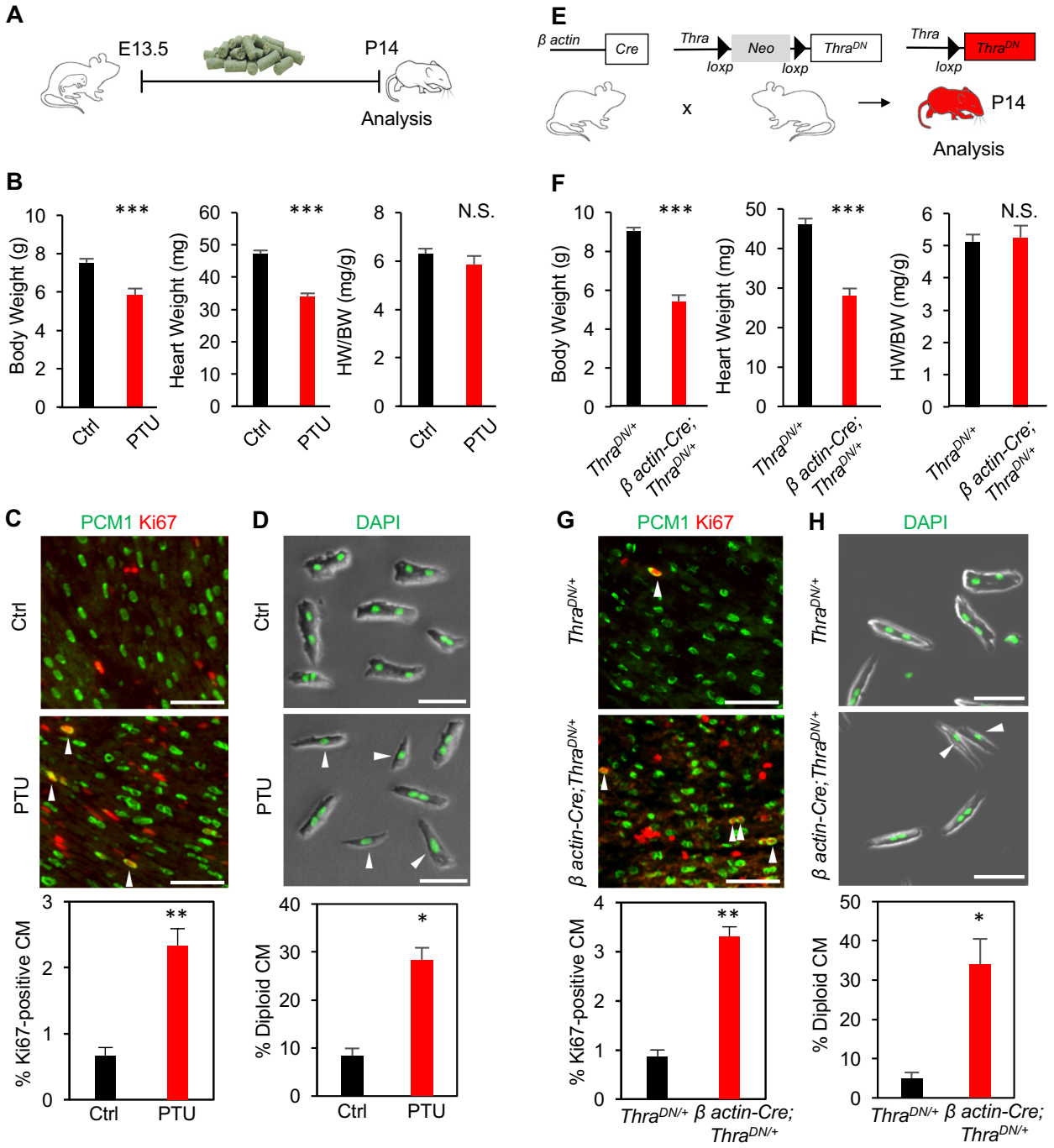

Figure S8. Global inhibition of thyroid hormone pathway activation delays postnatal mammalian cardiomyocyte (CM) cell cycle exit and retains more mononuclear diploid CMs in the heart. Schematics for (**A**) administrating a thyroid hormone synthesis inhibitor propylthiouracil (PTU) through diet and (**E**) genetic inactivation of thyroid hormone receptor by generating transgenic mice ubiquitously overexpressing a dominant negative (DN) thyroid hormone receptor *Thra*$^{DN/+}$. (**B**, **F**) Body weight (BW), heart weight (HW), and ratio of HW to BW of indicated mice (n=4 animals). (**C**, **G**) Representative images and quantification of proliferating CMs (n=3 animals). Ki67-positive cardiomyocytes are marked by arrowheads. (**D**, **H**) Morphology and nucleation analysis of CMs (n=3 animals). Arrowheads indicate mononucleated CMs. Values are reported as Mean ± SEM. * P<0.05, ** P<0.01, *** P<0.001. N.S., no significant difference. Scale bars, 100 μm.

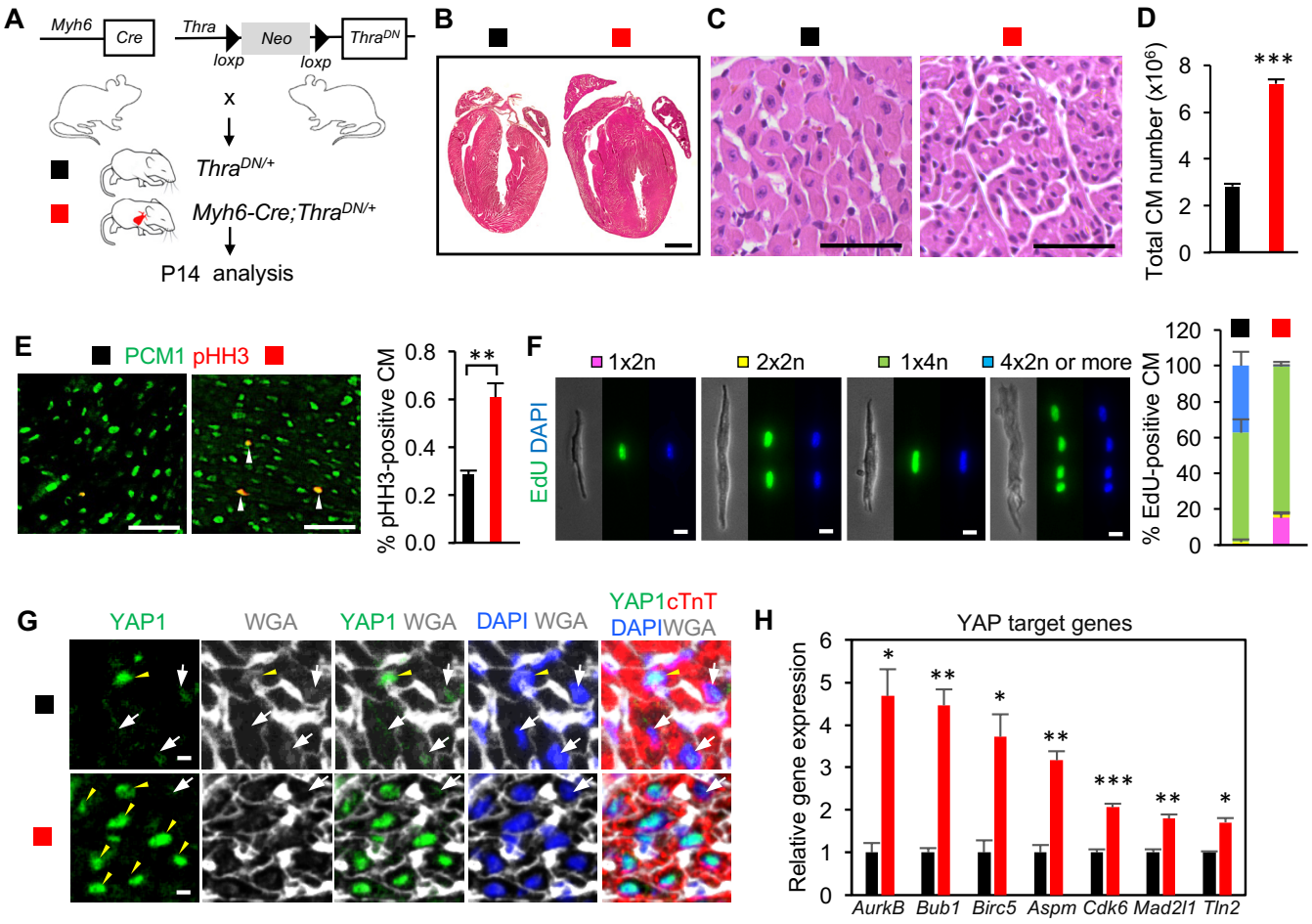

Figure S9. Cardiomyocyte (CM)-specific inactivation of thyroid hormone receptor enhances CM proliferation in neonatal mice. (**A**) Schematic for generating *Myh6-Cre; Thra*$^{DN/+}$ mice with CM-restricted expression of a dominant negative (DN) TRα and analyzing phenotypes at the postnatal day 14 (P14). (**B**) Low- and (**C**) high-magnification of H&E stained heart sections of control and mutant mice at P14. (**D**) Total CM number estimated by design-based stereological methods (n=3 hearts). (**E**) Representative images and quantifications of proliferating CMs that stained positive for phosphorylated histone H3 (pHH3). Arrowheads indicate proliferating CM (n=4 animals). (**F**) Nucleation and ploidy analysis of EdU-incorporated CMs. After EdU injection at P12 and P13, animals were harvested at P14 and CMs were dissociated for ploidy analysis. Representative images of EdU-positive diploid (1x2n), tetraploid (both 2x2n and 1x4n), polyploid (4x 2n or more) CMs are shown, and quantification results are presented on the right (n=4 animals). (**G**) Immunostaining of YAP and quantifications (n=4 animals). Yellow arrowheads indicate CMs with nuclear YAP and white arrow show CMs with no nuclear YAP stain. (**H**) Examination of YAP target gene expression in a RNA-seq analysis (n=3 hearts). Values are reported as Mean ± SEM. * P<0.05, ** P<0.01, *** P<0.001. Scale bars, 1 mm (**B**), 50 μm (**C**),100 μm (**D**), 20 μm (**E**), 10 μm (**F**, **G**).

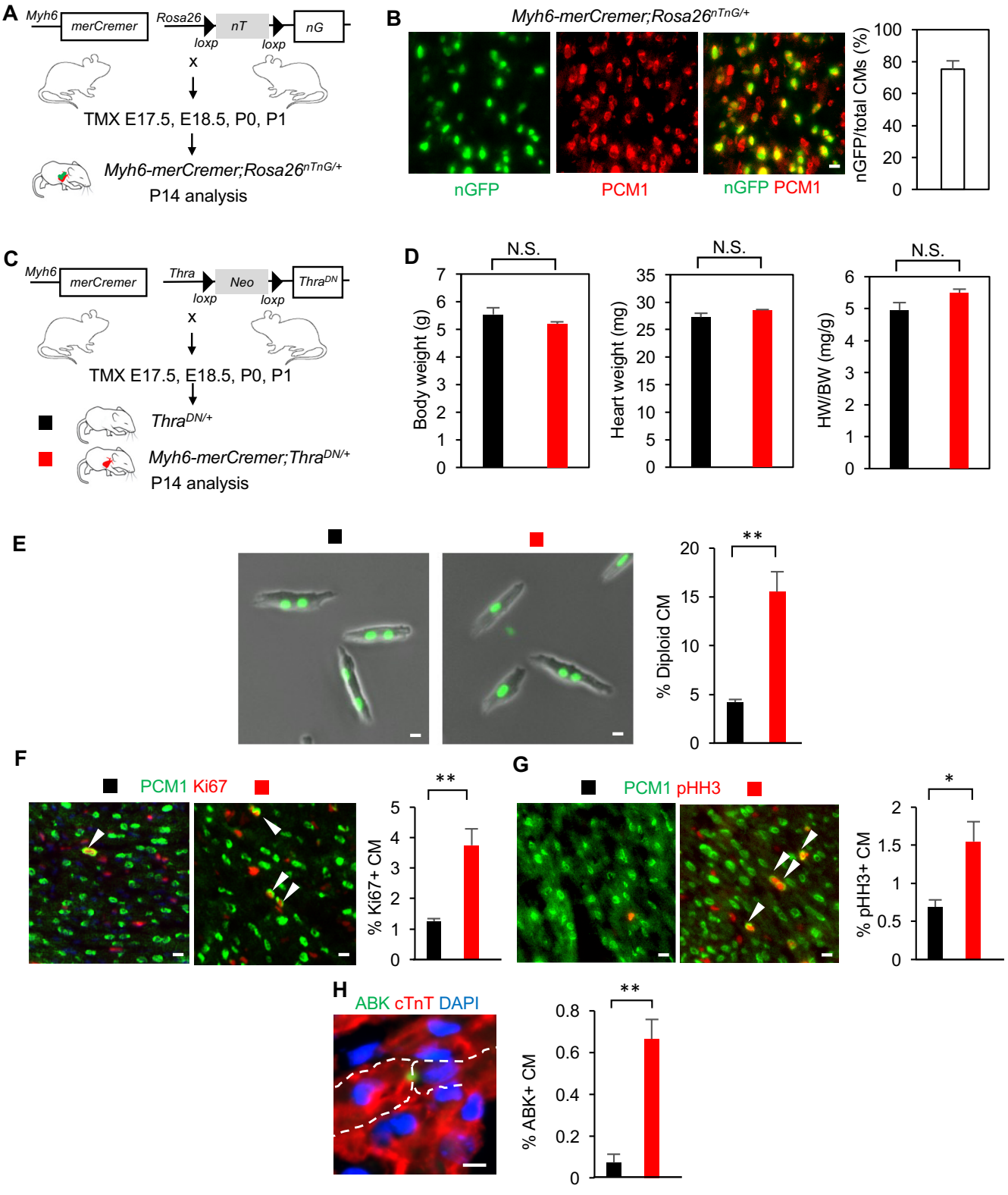
A
Myh6
merCremer
Rosa26
nT
nG
loxp
loxp
x
TMX E17.5, E18.5, P0, P1
Myh6-merCremer;Rosa26nTnG/+
P14 analysis
B
Myh6-merCremer;Rosa26nTnG/+
nGFP
PCM1
nGFP PCM1
nGFP/total CMs (%)
C
Myh6
merCremer
Thra
Neo
ThraDN
loxp
loxp
x
TMX E17.5, E18.5, P0, P1
ThraDN/+
Myh6-merCremer;ThraDN/+
P14 analysis
D
N.S.
Body weight (g)
Heart weight (mg)
HW/BW (mg/g)
E
% Diploid CM
F
PCM1 Ki67
% Ki67+ CM
G
PCM1 pHH3
% pHH3+ CM
H
ABK cTnT DAPI
% ABK+ CM

Figure S10. Perinatal inactivation of thyroid hormone receptor in cardiomyocytes (CMs) enhances CM proliferation in neonatal mice. (**A**) Schematic for testing the efficiency of a tamoxifen (TMX)-inducible cardiomyocyte Cre line in the perinatal window. (**B**) Nuclear GFP and PCM1 double positive CMs in 75% of all CMs (n=3 animals). (**C**) Schematic for generating *Myh6-merCremer;Thrα*$^{DN/+}$ mice with perinatal CM-restricted expression of a dominant negative (DN) TRα. (**D**) Measurements of body weight (BW), heart weight (HW), and HW/BW ratio (n=3 animals). (**E**) Morphology and ploidy analysis of CMs (n=3 animals). (**F**-**H**) CM proliferative activity analysis. Representative images and quantifications of proliferating CMs that stained positive for Ki67 (**F**), phosphorylated histone H3 (pHH3) (**G**) and Aurora B kinase (ABK) (**H**) (n=3 animals). Arrowheads indicate proliferating CM. In **H**, cardiomyocytes undergoing cytokinesis are outlined. Values are reported as Mean ± SEM. * P<0.05, ** P<0.01. No significant difference (N.S.). Scale bars, 10 μm.

A **Upregulated genes**

GSEA analysis (Hallmark pathways)

Pathway	P-value
G2M checkpoint	0
E2F targets	0
Estrogen response early	0
Mitotic spindle	0.041

GSEA analysis (KEGG pathways)

Pathway	P-value
Cell cycle	0

B **Downregulated genes**

GSEA analysis (Hallmark pathways)

Pathway	P-value
Oxidative phosphorylation	0
Adipogenesis	0
Myogenesis	0
Kras signaling	0
Xenobiotic metabolism	0
MTorc1 signaling	0.0011
Glycolysis	0.0023
Reactive oxygen species pathway	0.0054
Heme metabolism	0.0056
Myc targets	0.0067
Fatty acid metabolism	0.0082
Peroxisome	0.0099
Tnfa signaling via Nfkb	0.010
Allograft rejection	0.014
Inflammatory response	0.021
UV response	0.022
Interferon gamma	0.031
TGFbeta signaling	0.039

GSEA analysis (KEGG pathways)

Pathway	P-value
Oxidative phosphorylation	0
Citrate cycle (TCA cycle)	0
Parkinsons disease	0
Alzheimers disease	0
Huntingtons disease	0
Peroxisome	0
Proteasome	0
Cardiac muscle contraction	0
Ala, asp and glu metabolism	0
Val, Leu and Iso metabolism	0
Fructose and mannose metabolism	0
Propanoate metabolism	0
Glycerophospholipid metabolism	0.0019
Type I diabetes mellitus	0.0019
Pyruvate metabolism	0.0038
Glycolysis gluconeogenesis	0.0077
Nicotinate and nicotinamide metabolism	0.013
Protein export	0.014
Xenobiotic metabolism	0.015
Drug metabolism cytochrome P450	0.021
ABC transporters	0.027
FC epsilon RI signaling pathway	0.029
Glycerolipid metabolism	0.033

Ingenuity Pathway Analysis

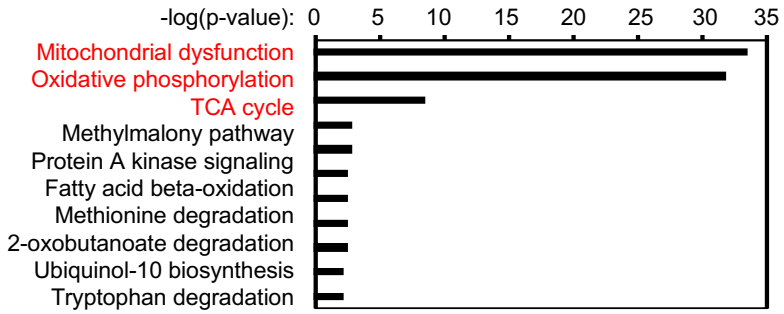

Figure S11. Bioinformatics analysis of biological pathways that change in the P14 hearts with deficiency in thyroid hormone signaling. For GSEA analysis, all pathways with a *P*-value less than 0.05 are listed. Note that the *P* value is assigned as 0 if *P*<0.001. For Ingenuity Pathway Analysis, top 10 most significant pathways are listed. The pathways shown in Fig. 3 are in red.

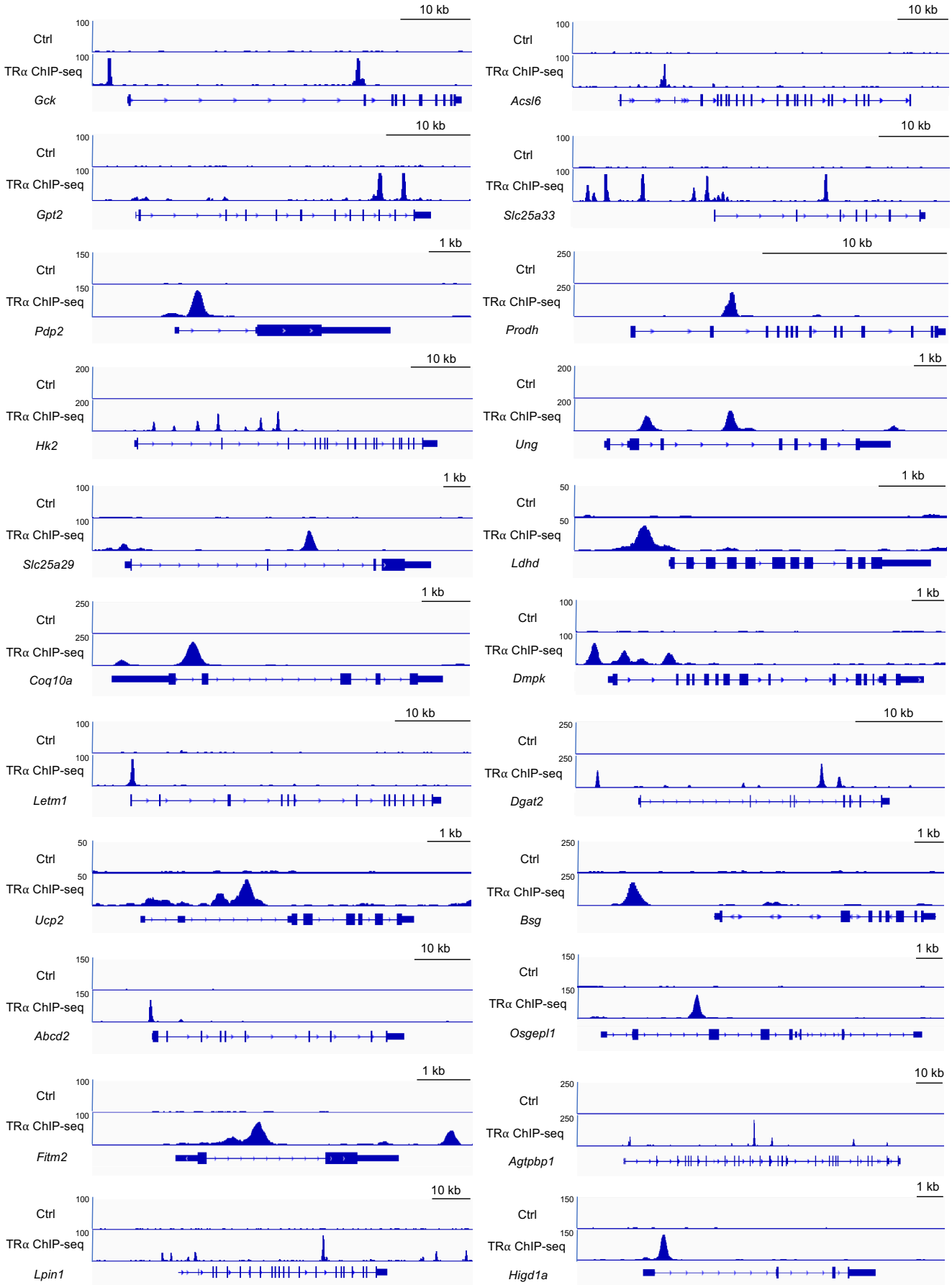
10 kb
Ctrl
TRα ChIP-seq
Gck
Acsl6
Gpt2
Slc25a33
1 kb
Pdp2
Prodh
Hk2
Ung
Slc25a29
Ldhd
Coq10a
Dmpk
Letm1
Dgat2
Ucp2
Bsg
Abcd2
Osgepl1
Fitm2
Agtpbp1
Lpin1
Higd1a

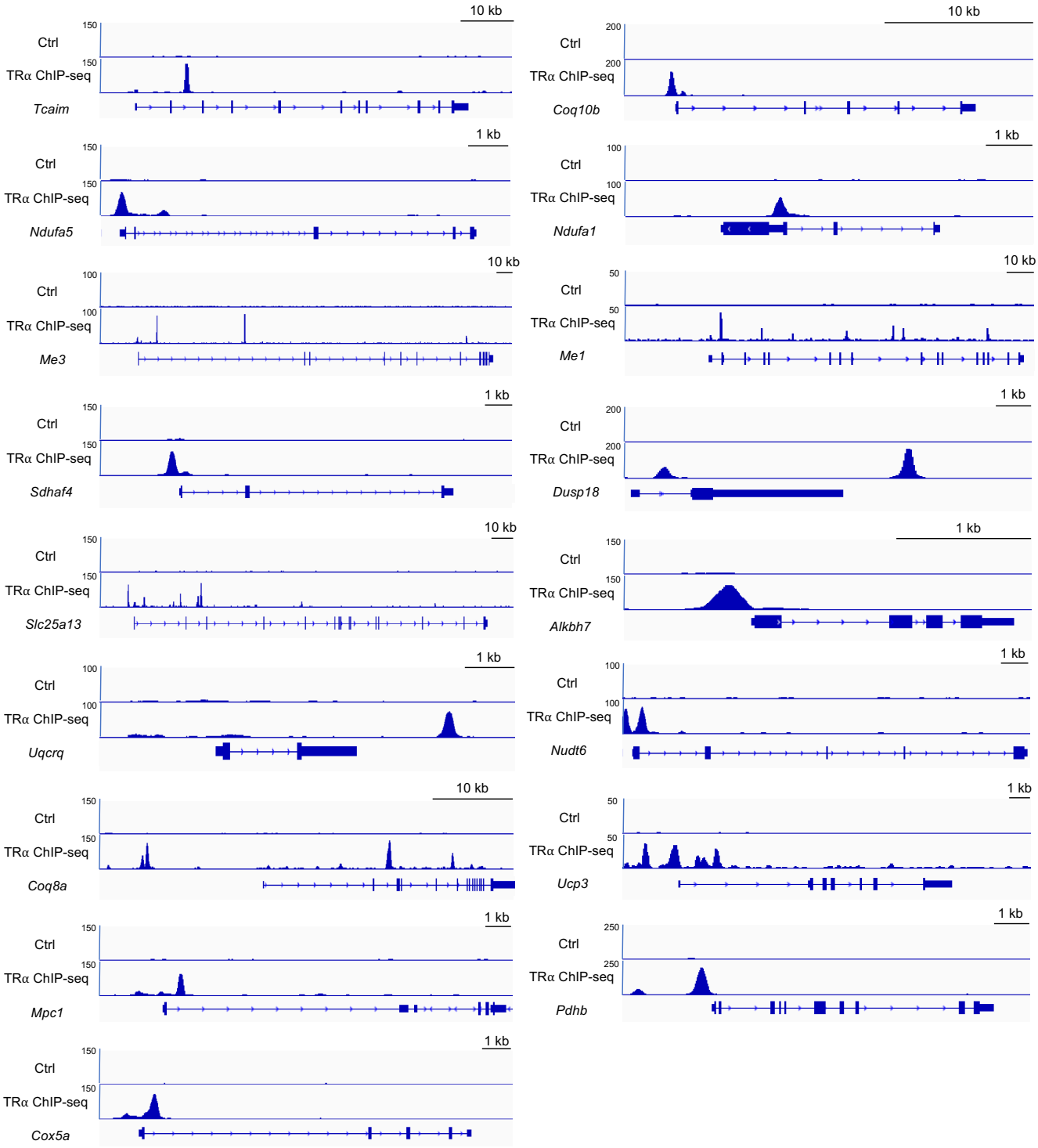

Figure S12. Examples of thyroid hormone receptor α (TRα) direct target genes. TRα chromatin immunoprecipitation-sequencing (ChIP-seq) analysis identifies TRα binding to the loci of many mitochondrial genes that are significantly downregulated in the mutant heart with deficiency in thyroid hormone signaling.

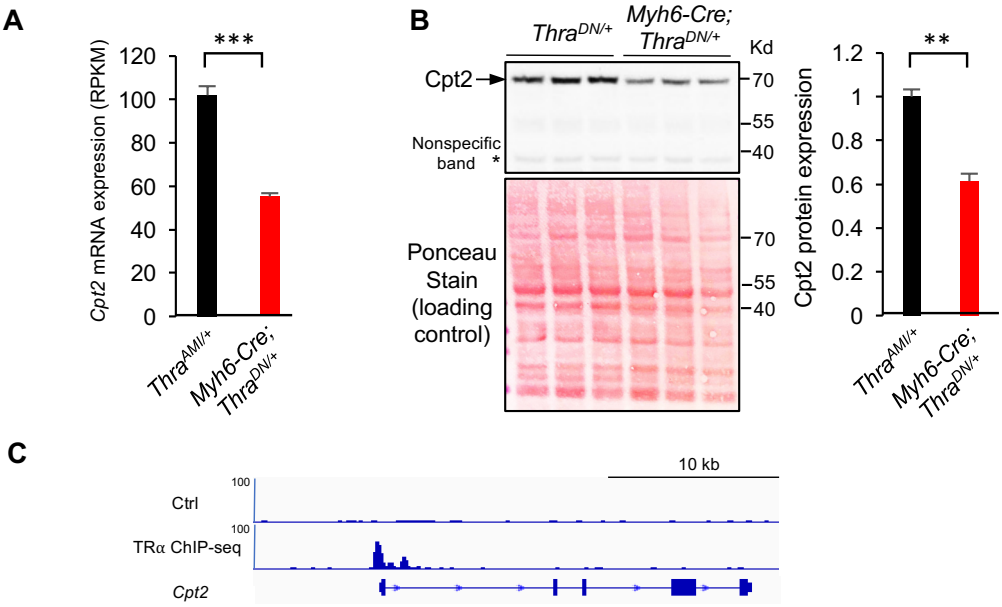

Figure S13. *Cpt2* is a direct target gene of thyroid hormone receptor α (TRα). (**A**) Cpt2 mRNA is down-regulated by ~50% in P14 *Myh6-Cre;Thra*$^{DN/+}$ hearts (n=3 hearts). The RNA-seq results in RPKM are presented. (**B**) Cpt2 protein is down-regulated by ~40% in P14 *Myh6-Cre;Thra*$^{DN/+}$ hearts as shown by western blot analysis using an anti-Cpt2 antibody (n=3 hearts). (**C**) TRα chromatin immunoprecipitation-sequencing (ChIP-seq) analysis identifies TRα binding to the promoter of *Cpt2* gene. Values are reported as Mean ± SEM. ** $P< 0.01$, *** $P< 0.001$.

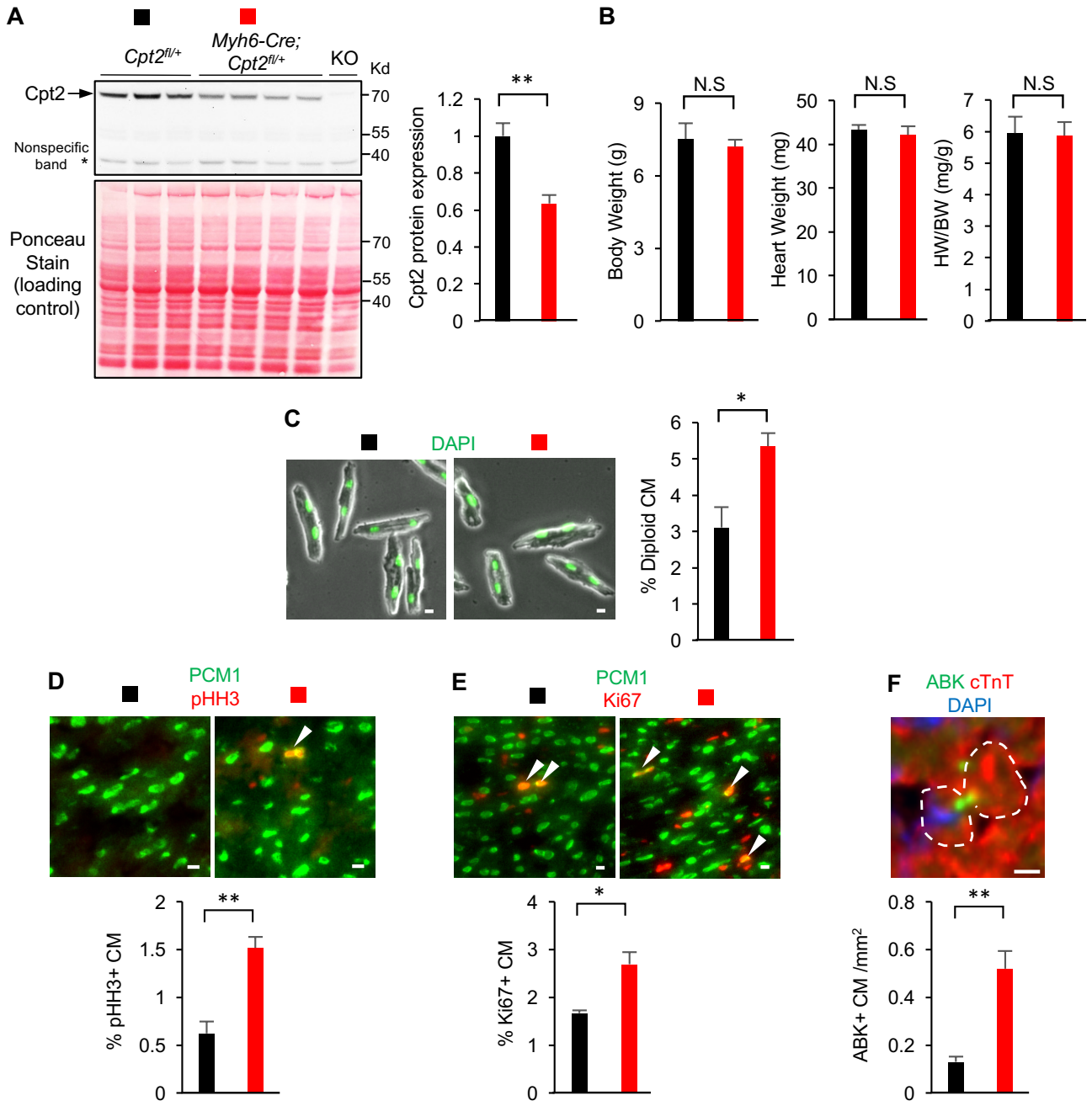

Figure S14. Cardiomyocyte (CM)-restricted heterozygous loss of *Cpt2* delays postnatal CM cell cycle exit. (**A**) Western blot analysis of Cpt2 protein expression in P14 hearts of indicated genotypes using an anti-Cpt2 antibody (n=3-4 hearts) (KO stands for *Myh6-Cre;Cpt2*$^{fl/fl}$). (**B**) Measurements of body weight (BW), heart weight (HW), and HW/BW ratio (n=3-5 animals). (**C**) Morphology and nucleation analysis of CMs (n=3 animals). (**D-F**) CM proliferative activity analysis. Representative images and quantifications of proliferating CMs that stained positive for phosphorylated histone H3 (pHH3) (**D**), Ki67 (**E**) and Aurora B kinase (ABK) (**F**) (n=3-5 animals). Arrowheads indicate proliferating CM. Values are reported as Mean ± SEM. * P<0.05, ** P<0.01. N.S., no significant difference. Scale bars, 10 μm.

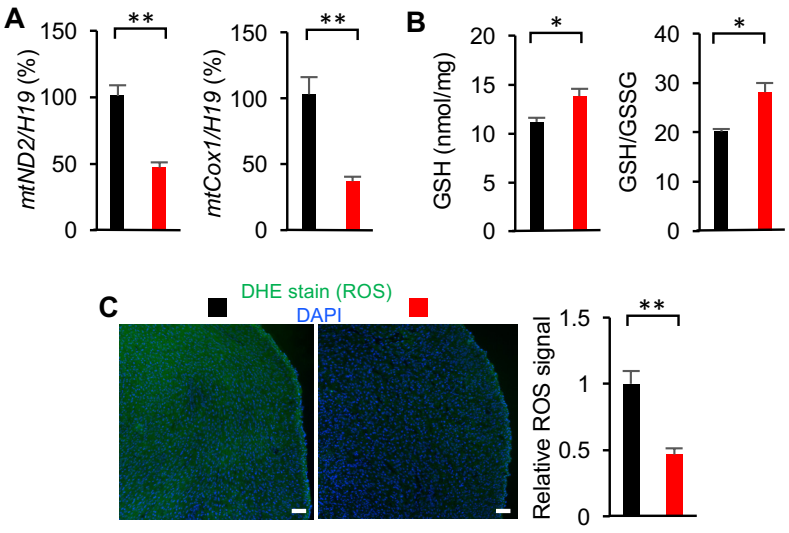

Figure S15. Cardiomyocytes (CM) with deficiency in thyroid hormone signaling show reduced reactive oxygen species (ROS) in neonatal mice. (**A**) Mitochondrial DNA analysis (n=4 hearts). (**B**) GSH and GSH:GSSG measurement (n=3 hearts). (**C**) Reactive oxygen species determination on freshly frozen heart sections (n=3 hearts). All control and mutant heart sections are placed on the same glass, stained and imaged exactly in the same manner. Values are reported as Mean ± SEM. * $P<0.05$, ** $P<0.01$. Scale bars, 100 μm.

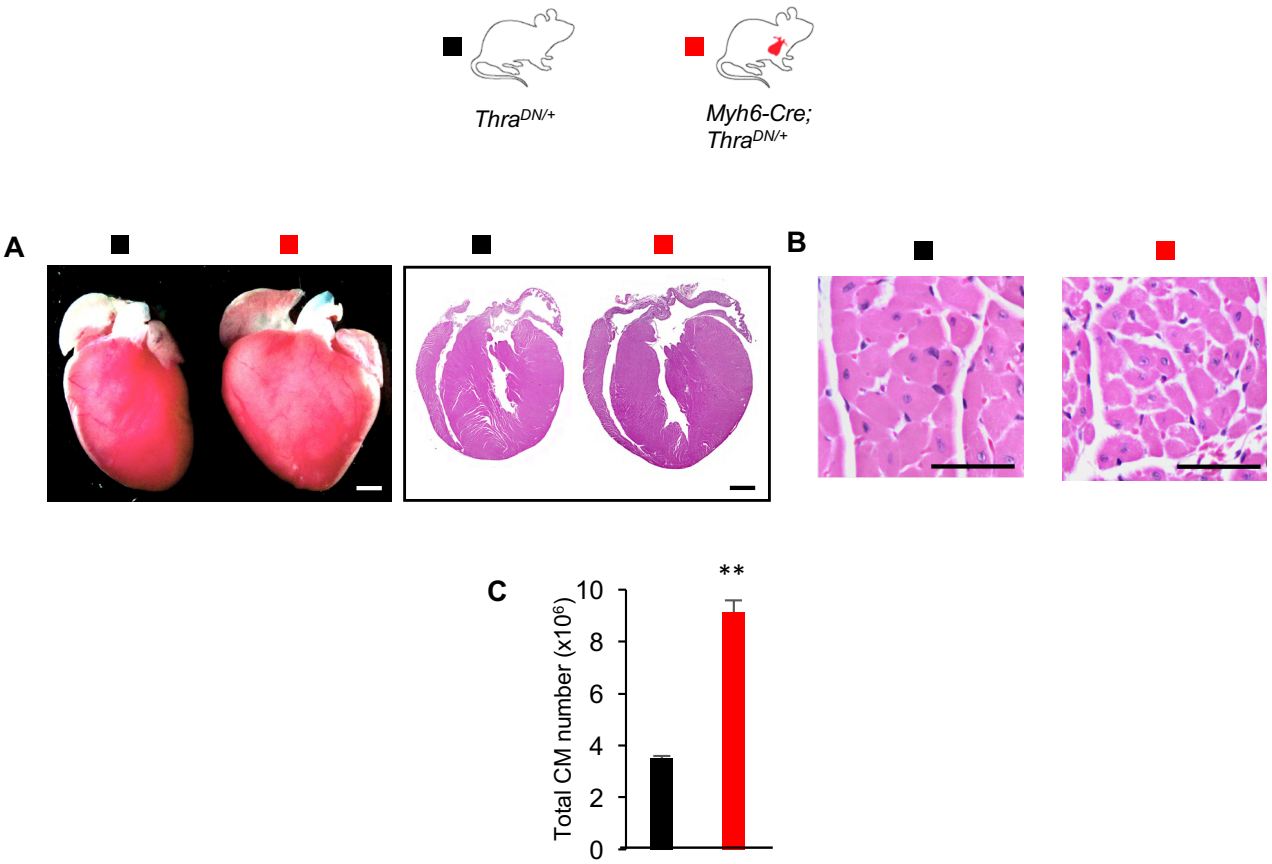

Figure S16. Adult mice with cardiomyocytes (CM) deficient in thyroid hormone signaling preserve the phenotypes of enlarged heart size, reduced CM cell size and more CMs. (**A**) Low-magnification whole-mount and cross-section views. (**B**) High-magnification views showing smaller CM cell size in the mutant mice. Mutant and control littermate controls were analyzed at 13 weeks old. (**C**) Total CM number estimated by design-based stereological methods (n=3 hearts). Scale bars, 1 mm (**A**), 50 μm (**B**). ** *P*<0.01.

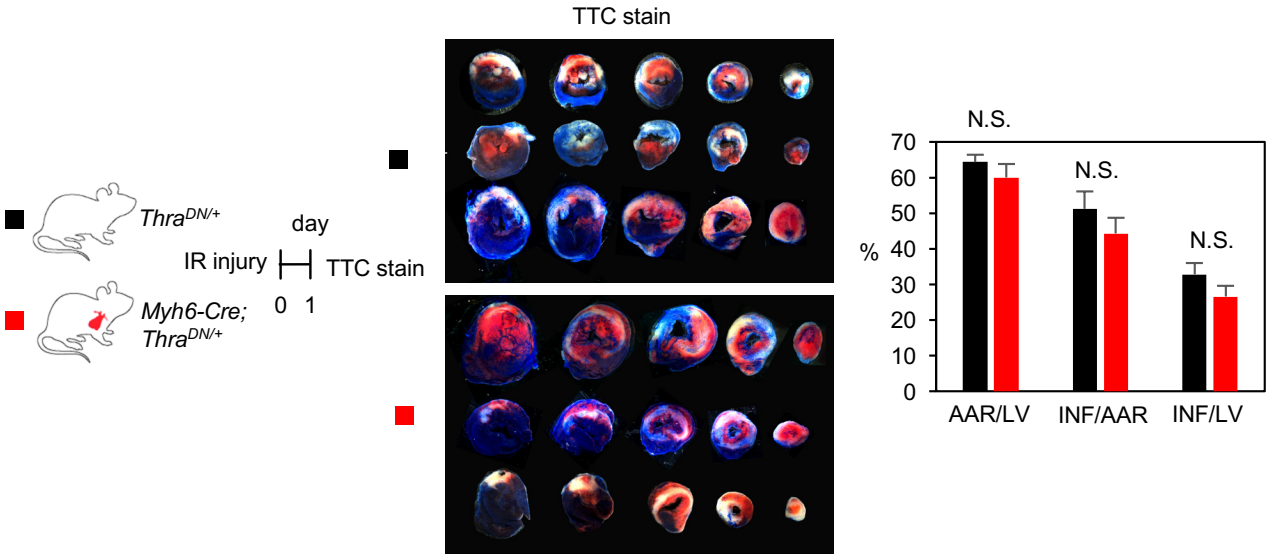

Figure S17. Mice with cardiomyocytes (CM) deficient in thyroid hormone signaling show a comparable extent of injury 24 hours after myocardial ischemia reperfusion (IR). Schematic of the experimental timeline after IR injury to analyze area of risk and injury. Tetrazolium chloride (TTC) stains 24 hours after IR reveal comparable levels of injury between mutant and control hearts (n=11 control and 10 mutant animals). No statistical difference was found. White, infarct area (INF). Red, the myocardial area with no perfusion, or area at risk (AAR). Blue, the myocardial area with normal perfusion. LV, left ventricle. TTC stains of three control and three mutant hearts are shown. N.S., not significant.

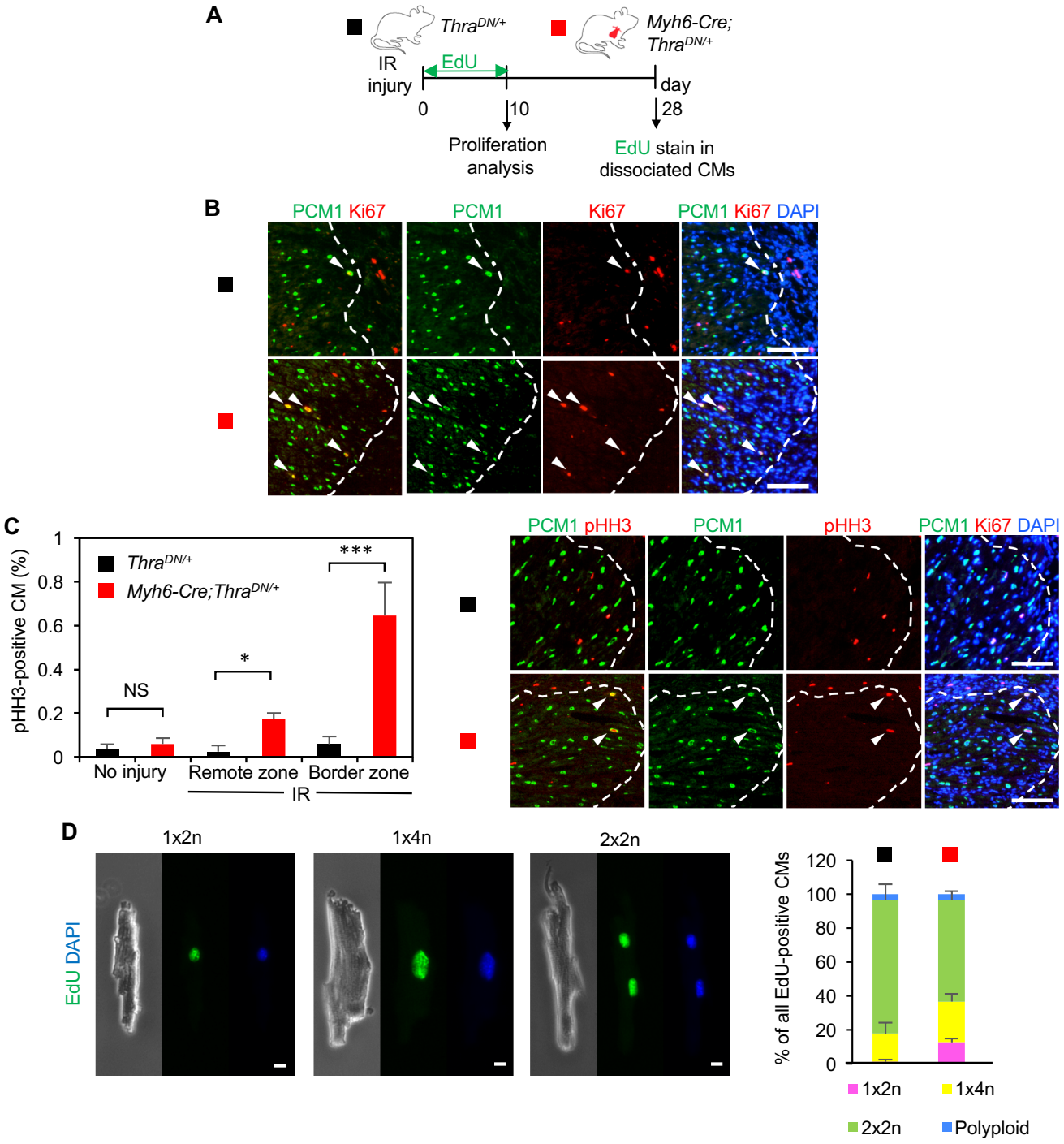

Figure S18. Nucleation and ploidy analysis of EdU-incorporated cardiomyocytes (CMs) after injury. (**A**) Schematic of the experimental timeline after myocardial ischemia-reperfusion (IR) injury. EdU is injected daily in the first ten days after injury. Dissociated CMs are analyzed 28 days after IR. (**B, C**) CM proliferation analysis 10 days after myocardial injury. (B) Representative images of Ki67- positive CMs around the injury border zone for Fig. 4D. (C) Quantification and Representative images of phospho-histone H3 (pHH3)-positive CMs in the hearts with no injury (n=3-4 animals) or the hearts after IR injury (n=4-5 animals). Dash lines mark the border of injury whereas arrowheads show proliferating CMs. (**D**) Representative images of EdU-positive diploid (1x2n) and tetraploid (both 2x2n and 1x4n) CMs are shown. Quantification results are presented (n=4 animals). Values are reported as Mean ± SEM. * P<0.05, *** P<0.001. Scale bars, 100 μm (**B**, **C**) and 10 μm (**D**).

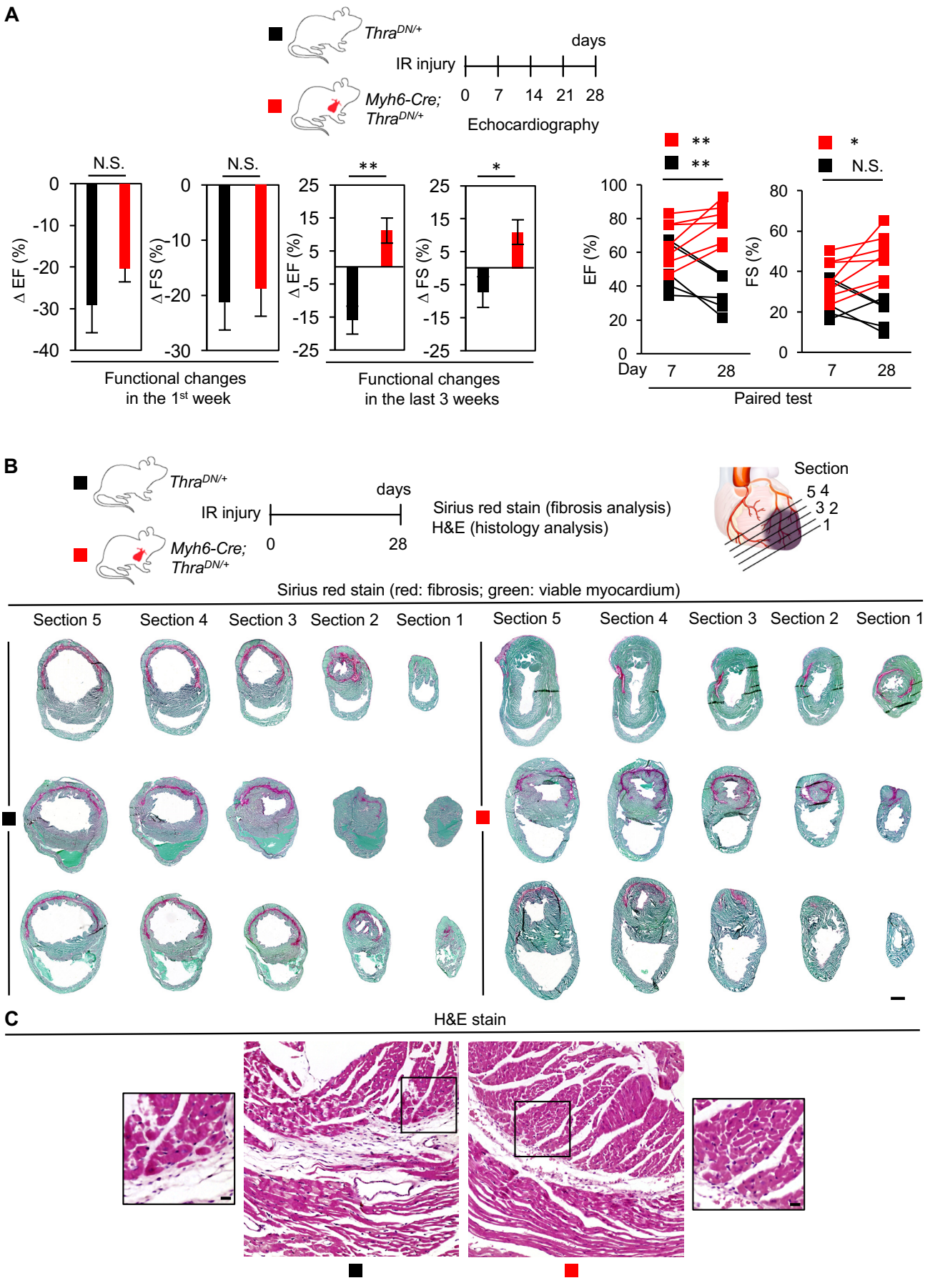
A
Thra^DN/+
Myh6-Cre; Thra^DN/+
days
IR injury
0 7 14 21 28
Echocardiography
N.S.
N.S.
**
*
Δ EF (%)
Δ FS (%)
Functional changes in the 1st week
Functional changes in the last 3 weeks
EF (%)
FS (%)
Day
Paired test
B
Thra^DN/+
Myh6-Cre; Thra^DN/+
IR injury
days
0
28
Sirius red stain (fibrosis analysis)
H&E (histology analysis)
Section
5 4
3 2
1
Sirius red stain (red: fibrosis; green: viable myocardium)
Section 5
Section 4
Section 3
Section 2
Section 1
C
H&E stain

Figure S19. Mice with cardiomyocytes (CM) deficient in thyroid hormone signaling show functional increases and reduced fibrosis 28 days after myocardial ischemia reperfusion (IR). (**A**) Schematic of the experimental timeline after IR injury to analyze cardiac functions by echocardiography. Analyses of ejection fraction (EF) and fraction shortening (FS) of individual animals. Values are mean ± SEM (n=5 control and 7 mutant animals). * denotes $P<0.05$ and ** denotes $P<0.01$. N.S., not significant. (**B**) Schematic of the experimental timeline after IR injury to analyze fibrosis. The heart is sectioned every 500 μm from the apex. Sirius red stains of three control and three mutant hearts are shown. Note that most injured hearts from control mice have dilated myocardium and larger left ventricular lumens. (**C**) H&E stained hearts 28 days after IR, with high-magnification views of the boxed areas shown on the two sides. Scale bars, 1 mm (**B**), 20 μm (**C**).

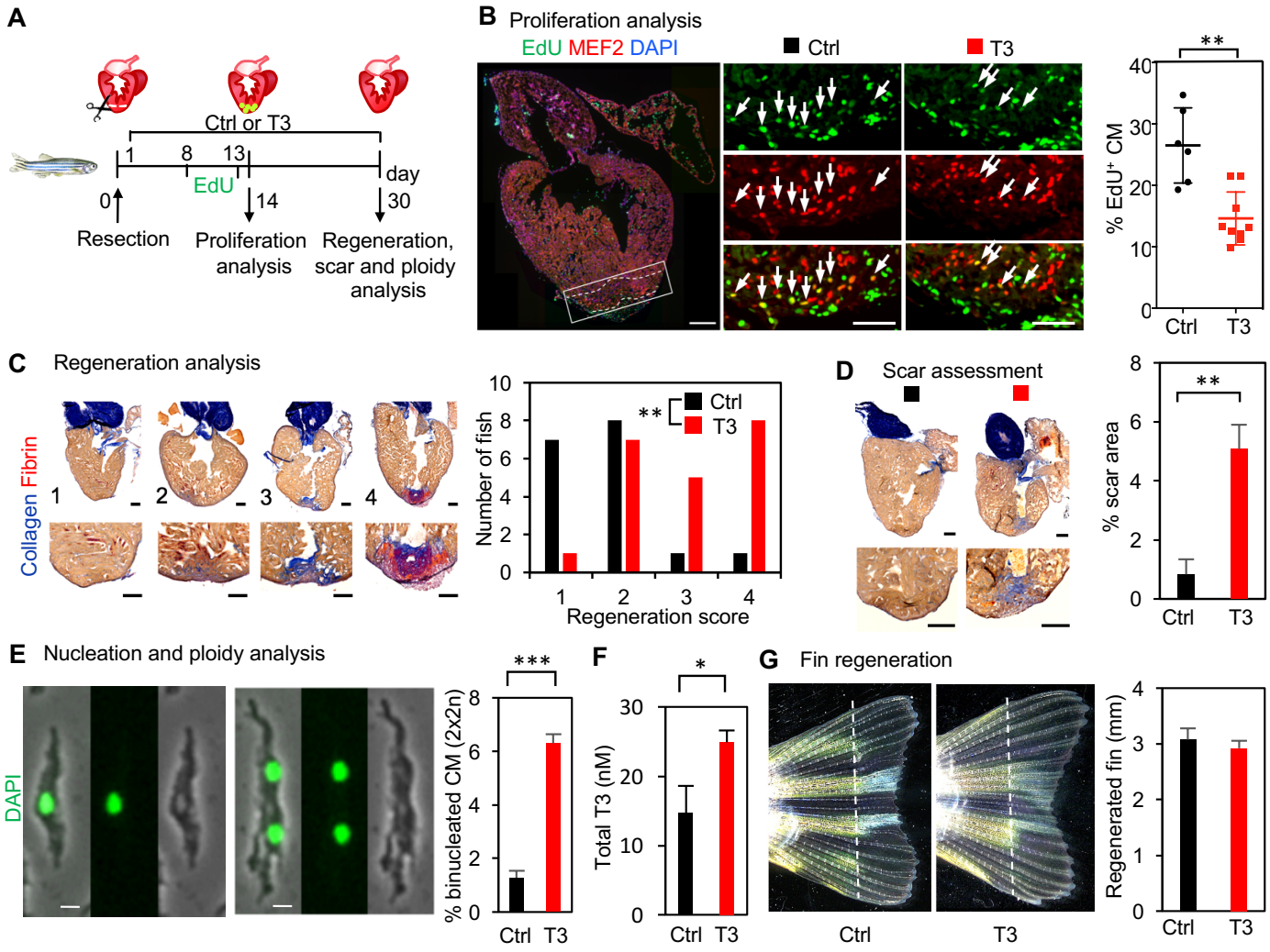

Figure S20. Exogenous thyroid hormone inhibits cardiomyocyte (CM) proliferation and heart regeneration in adult zebrafish. (**A**) Schematic of zebrafish heart injury and analysis. (**B**) Proliferation analysis 14 days after injury. CM nuclei are stained positive for MEF2. EdU-incorporated CMs are examined at the border zone within the area 100 μm from the injury site, as marked by two dash lines in a boxed area. Magnifications of the border zone are shown in the middle with arrows pointing at EdU-positive CMs. Quantifications are presented (n=6-9 animals). (**C**) Heart regeneration analysis 28 days after injury. Acid fuchsin orange (AFOG) stains reveal collagen in blue and fibrin in red. The extent of regeneration is scored as: 1, complete regeneration with no visible collagen or fibrin; 2, almost complete regeneration with small but visible collagen; 3, partial regeneration with abundant collagen; 4, little regeneration with prominent collagen and fibrin stains. Quantifications are shown on the right (control, n=17 and T3-treated, n=21). (**D**) Scar analysis 28 days after injury. Presented are representative images of AFOG-stained heart sections with the fibrotic scar in blue, and quantifications of the scar area in the ventricle of control (n=17) and T3-treated (n=21) fish. (**E**) Nucleation and ploidy analysis of CMs from control and T3-treated fish 28 days after injury (n=3 animals). (**F**) Measure of serum total T3 levels (n=5 animals). (**G**) Fin regeneration is not affected by the same dose of T3 treatment (n=8 control and 7 T3-treated fish). Dash lines indicate the amputation plane. Values are reported as Mean ± SEM. * P<0.05, ** P<0.01, *** P<0.001. Scale bars, 100 μm (**B**-**D**) and 10 μm (**E**).

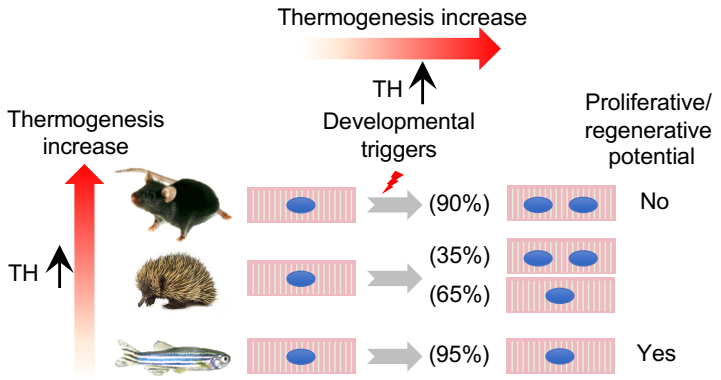

Fig. S21. A proposed model about the role of thyroid hormones in heart regeneration. Increased levels of thyroid hormones (THs) inhibit cardiomyocyte proliferative and regenerative potential during the acquisition of endothermy in evolution and development.

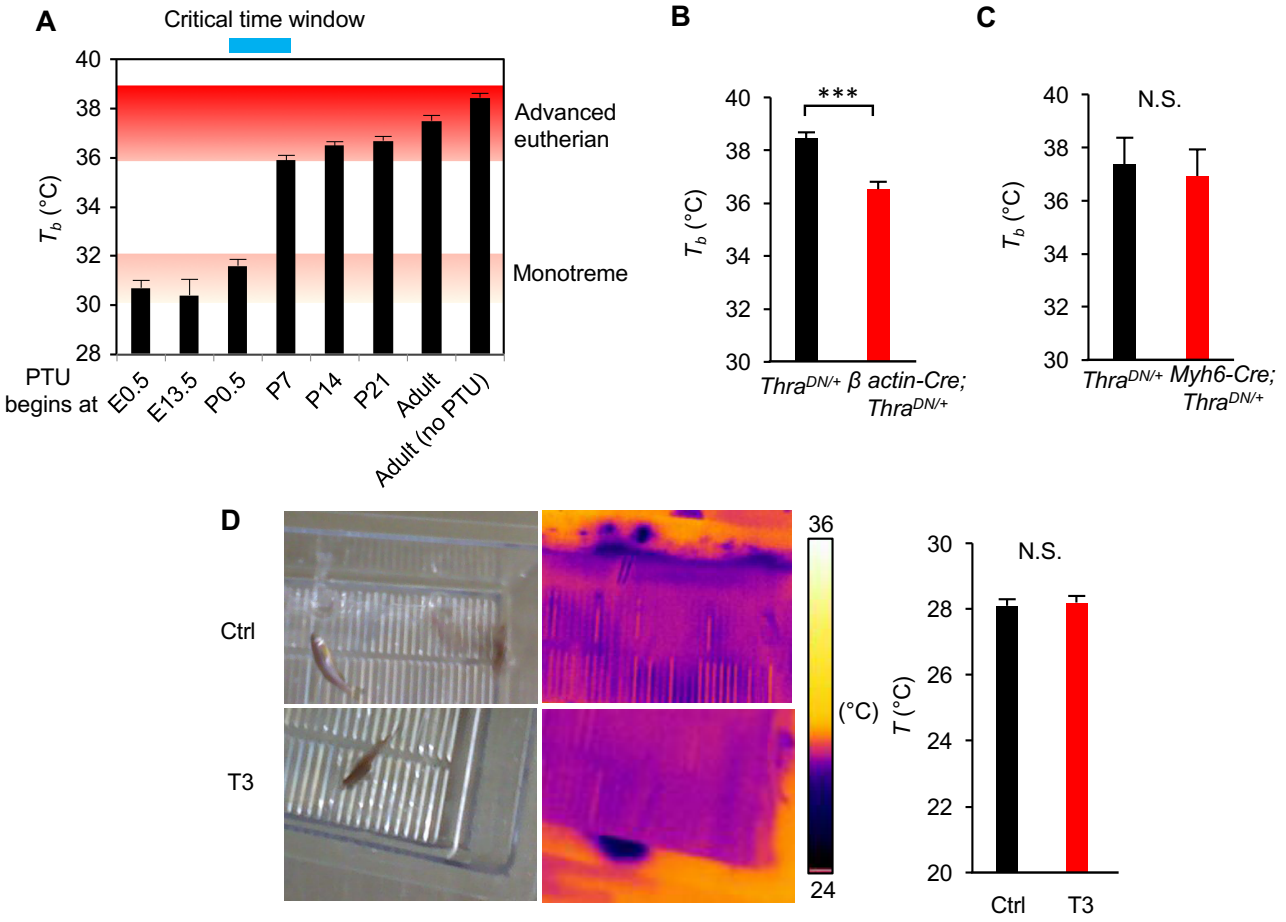

Figure S22. Effect of thyroid hormone pathway manipulation on body temperature control. (**A**) Critical postnatal time window of body temperature regulation by thyroid hormones (TH). To inhibit TH synthesis, mice were only given food chows contain a TH synthesis inhibitor PTU at different developmental stages. Rectal temperature (T_b) was measured at least two months after PTU administration. Values are reported as Mean ± SEM (n=3 independent experiments with a cohort of 3-10 animals per experiment). The ranges of monotreme and advanced eutherian T_b are shown. (**B**) Significant lower rectal temperature in mutant mice with global expression of a dominant negative thyroid hormone receptor α (n=8 animals). (**C**) Measurement of rectal temperature of control and mutant mice with cardiomyocyte-specific expression of a dominant negative thyroid hormone receptor α (n=3 animals). (**D**) Measurement of zebrafish body temperature using an infrared red camera (bright field views on the left and infrared red images on the right). Quantification of control and T3-treated fish body temperature (control or T3 treatment for seven days) (n=5 animals). Note the ambient temperature of the zebrafish facility is 28°C. Values are reported as Mean ± SEM. *** P<0.001. N.S., no significant difference.

Table S2. Distribution of cardiomyocytes by ploidy classes in vertebrates (%).

Animal Species	Latin name	Diploid	Tetraploid		Multiploid			*n*	Source or Ref.
		1x2n	1x4n	2x2n	2x4n	4x2n	Others		
Pisces									
Zebrafish	*Danio rerio*	99	0.3	0.7	0	0	0	7	(4)
Amphibia									
Red-spotted newt	*Notophthalmus viridescens*	98.3±0.6	0.9±0.1	0.8±0.7	0	0	0	3	(38)
Western toad	*Anaxyrus boreas*	87.7±3.3	8.5±1.7	2.2±1.0	0.47±0.5	0	1.3±0.4	3	Museum of Vertebrate Zoology
African clawed frog	*Xenopus laevis*	94.7±1.1* (1x4n)	3.1±1.5* (1x8n)	1.9±0.5* (2x4n)	0.2±0.2* (2x8n)	0 (4x4n)	0.2±0.2*	3	Heald Lab
Reptilia									
Western fence lizard	*Sceloporus occidentalis*	77.1±1.6	8.9±1.5	10.0±0.8	1.0±0.5	0.2±0.2	2.9±0.6	3	Museum of Vertebrate Zoology
Green anole	*Anolis carolinensis*	89.8±1.5	5.5±1.1	4.3±0.1	0	0	0.5±0.5	2	Wilson-Rawls Lab
Mammalia									
Monotremata									
Platypus	*Ornithorhynchus anatinus*	55.8±5.4	6.8±2.2	29.4±2.6	3.7±2.3	0.9±0.6	3.0±1.5	3	Grutzner Lab
Short-beaked echidna	*Tachyglossus aculeatus*	59±4.1	10.1±6.4	25.9±3.0	2.3±1.2	0	1.7±0.9	3	Grutzner Lab
Cingulata									
Naked-tailed armadillo	*Cabassous unicinctus*	52.3	1.7	39.6	0.9	0.4	5.1	1	Museum of Vertebrate Zoology
Pilosa									
Silky anteater	*Cyclopes didactylus*	60.3	2.2	26.8	1.3	0.9	8.5	1	Museum of Vertebrate Zoology
Lesser anteater	*Tamandua tetradactyla*	55.9±0.9	2.2±0.2	32.5±1.6	2.5±2.5	0.4±0.3	4.5±3.2	2	Museum of Vertebrate Zoology
Brown-throated three-toed sloth	*Bradypus variegatus*	33.3±1.8	4.6±1.6	50.5±3.5	0.75±0.75	2.7±0.4	7.8±3.8	2	Museum of Vertebrate Zoology
Didelphimorphia									
Brown-eared woolly opossum	*Caluromys lanatus*	27.1	7.5	47.2	4.2	2.3	11.7	1	Museum of Vertebrate Zoology
Chiroptera									
Little brown bat	*Myotis lucifugus*	43.8±1.3	2.4±0.7	51.9±0.4	0.2±0.2	0.2±0.2	1.6±0.6	3	Field Lab
Egyptian fruit bat	*Rousettus aegyptiacus*	33.8±3.3	1.9±0.7	57.1±2.0	2.4±0.6	1.6±0.6	3.0±1.2	4	Yartsev Lab
Eulipotyphla									
Etruscan shrew	*Suncus etruscus*	12.8±0.4	1.6±0.3	65.6±2.0	2.2±0.5	4.9±0.8	13.0±2.2	3	Boyden Lab
Rodentia									
Mouse (CD1 strain)	*Mus musculus*	9.4±1.6	2.4±1.1	77.0±4.9	1.5±0.9	1.8±1.0	7.8±4.0	3	Huang lab
Guinea pig	*Cavia porcellus*	16.3±0.1	0.5±0.4	74.8±2.7	2.5±1.2	1.2±1.0	4.9±0.8	2	Buffenstein Lab
Mongolian gerbil	*Meriones unguiculatus*	14.9±2.2	3.8±0.5	60.0±5.8	6.7±3.4	3.1±1.8	11.4±3.0	3	Buffenstein Lab
Spiny mouse	*Acomys cahirinus*	19±0.7	4.3±0.8	65.4±2.8	1.8±1.1	1.7±0.6	7.8±0.6	3	Buffenstein Lab, Maden Lab
Cactus mouse	*Peromyscus eremicus*	30.4±2.0	37±0.8	56.4±2.4	2.4±1.0	1.0±0.6	6.2±2.0	3	Buffenstein Lab
Rat	*Rattus norvegicus*	13	3	79.3	2.3	2.4	0	3	(39)
Afghan vole	*Blanfordimys afghanus*	17.7	0	80	0	2.3	0	3	(39)
Afghan mouse-like hamster	*Calomyscus mystax*	11.7	8.3	73.2	2	4.8	0	3	(39)
Artiodactyla									
Bowhead whale	*Balaena mysticetus*	43.6±0.5	7.0±1.2	39.0±2.0	1.6±0.5	0.5±0.3	8.3±1.2	3	UA Museum of the North
Sperm whale	*Physeter macrocephalus*	22.4	6.5	55.7	2	3	10.4	1	UA Museum of the North
Calf	*Bos taurus*	10	2.7	65.3	1.7	17	3.3	3	(39)
Barbary sheep	*Ammotragus lervia*	12	1	65.3	1	20.7	0	2	(39)
Swine	*Sus scrofa*	6.3	5.3	28	3	45	12.3	3	(39)
David's deer	*Elaphurus davidianus*	9	0	72.6	0	18.3	0	2	(39)
Reindeer	*Rangifer tarandus*	6.7	2	70.3	1.7	19.3	0	2	(39)
Lagomorpha									
Rabbit	*Oryctolagus cuniculus*	11.7	2.7	67	0.3	18.3	0	3	(39)
Perissodactyla									
Wild horse	*Equus przewalskii*	8.3	0	83	0	8.7	0	1	(39)
Domestic horse	*Equus caballus*	10.3	0	75	0	14.7	0	3	(39)

Table S2. continued.

Animal Species	Latin name	Diploid	Tetraploid		Multiploid			*n*	Ref.
		1x2n	1x4n	2x2n	2x4n	4x2n	Others		
Carnivora									
Coyote	*Canis latrans*	4	2.7	90.3	3	0	0	1	(39)
Gray wolf	*Canis lupus*	6.7	3	85	0	5.3	0	3	(39)
Arctic fox	*Vulpes lagopus*	13.1	3.9	80.9	2.1	0	0	3	(39)
Red fox	*Vulpes vulpes*	6.4	0	88.4	0	5.2	0	3	(39)
Least weasel	*Mustela nivalisa*	4.7	0	90.3	0	5	0	2	(39)
Primates									
Human	*Homo sapiens*	4	25.7	33.7	21.3	0	15.3	3	(39)

* Note the tetraploidy of African clawed frogs (i.e. their non-cardiomyocytes are tetraploid). The nucleation and ploidy data for this species are shown in parentheses below.

Table S3. Physiological features of vertebrates.

Animal Species (Latin name)	BT (°C)	Ref.	Standard Metabolism (watt/kg^0.75)	Ref.	BW (kg)	Ref.	Systolic BP (mmHg)	Ref.	Diastolic BP (mmHg)	Ref.	Heart rate (/min)	Ref.
Pisces												
Zebrafish *(Danio rerio)*			0.091	(40)	0.000481	(40)					130	(40)
Amphibia												
Red-spotted newt *(Notophthalmus viridescens)*			0.164	(41)	0.0021	(41)						
Western toad *(Anaxyrus boreas)*			0.0456	(42)	0.0402						35	(42)
African clawed frog *(Xenopus laevis)*			0.0948	AnAge	0.0636	AnAge					37	(43)
Reptilia												
Western fence lizard *(Sceloporus occidentalis)*			0.34	(44)	0.0126	(44)					96	(45)
Green anole *(Anolis carolinensis)*			0.37	(46)	0.0057	(46)						
Mammalia												
Monotremata												
Platypus *(Ornithorhynchus anatinus)*	32	(47)	1.89	AnAge	1.03	AnAge					185	(48)
Short-beaked echidna *(Tachyglossus aculeatus)*	30.7	AnAge	0.98	AnAge	2.909	AnAge	123	(48)	96	(48)	59	(48)
Cingulata												
Naked-tailed armadillo *(Cabassous unicinctus)*			1.68	AnAge								
Pilosa												
Silky anteater *(Cyclopes didactylus)*	33	AnAge	1.85	AnAge	0.24	AnAge					60	(48)
Lesser anteater *(Tamandua tetradactyla)*	33.5	AnAge	1.95	AnAge	3.5	AnAge					80	(48)
Brown-throated three-toed sloth *(Bradypus variegatus)*	32.8	(49)			4.14	PanTHERIA	139	(50)			85	(50)
Chiroptera												
Little brown bat *(Myotis lucifugus)*	32	AnAge	2.42	AnAge	0.0058	AnAge	105	(51)	40	(51)	400	(51)
Egyptian fruit bat *(Rousettus aegyptiacus)*	33.4	AnAge	2.9	AnAge	0.146	AnAge						
Eulipotyphla												
Etruscan shrew *(Suncus etruscus)*	36	AnAge	3.98	(52)	0.002	AnAge					835	(50)
Rodentia												
Mouse *(Mus musculus)*	36.9	AnAge	3.33	(53)	0.021	AnAge	116	(54)	82	(54)	580	(53)
Guinea pig *(Cavia porcellus)*	39	AnAge	3.32	(7)	0.64	AnAge	83.8	(54)	50	(54)	273	(50)
Mongolian gerbil *(Meriones unguiculatus)*	36.35	AnAge			0.04	AnAge						
Spiny mouse *(Acomys cahirinus)*	37.5	AnAge	2.78	AnAge	0.042	AnAge						
Cactus mouse *(Peromyscus eremicus)*	36.6	AnAge	3.13	(*55*)	0.0215	(*55*)						
Rat *(Rattus norvegicus)*	37.1	AnAge	3.37	(53)	0.28	AnAge	125	(52)	99	(52)	320	(54)

Table S3. continued.

Animal Species (Latin name)	BT (°C)	Ref.	Standard Metabolism (watt/kg^0.75)	Ref.	BW (kg)	Ref.	Systolic BP (mmHg)	Ref.	Diastolic BP (mmHg)	Ref.	Heart rate (/min)	Ref.
Rodentia												
Afghan vole *(Blanfordimys afghanus)*												
Afghan Mouse-like hamster *(Calomyscus mystax)*					0.024	AnAge						
Artiodactyla												
Cattle *(Bos taurus)*	38	AnAge	3.65	(7)	347	AnAge	160	(56)	110	(56)	80	(57)
Barbary sheep *(Ammotragus lervia)*					92	AnAge						
Swine *(Sus scrofa)*	39						125	(56)	85	(56)	84	(50)
David's deer *(Elaphurus davidianus)*					186.5	AnAge						
Reindeer *(Rangifer tarandus)*	37.2	AnAge			85	AnAge						
Sperm whale *(Physeter macrocephalus)*	37	(58)			28500	AnAge						
Bowhead whale *(Balaena mysticetus)*	33.6	(59)			100000	AnAge						
Lagomorpha												
Rabbit *(Oryctolagus cuniculus)*	39	AnAge	3.56	(7)	1.8	AnAge	110	(56)	77	(56)	251	(50)
Perissodactyla												
Wild horse *(Equus przewalskii)*												
Domestic horse *(Equus caballus)*	38.3	AnAge			300	AnAge	115	(56)	80	(56)	47	(50)
Carnivora												
Coyote *(Canis latrans)*	37	AnAge	3.42	AnAge	10.148	AnAge						
Gray wolf *(Canis lupus)*	38.3	AnAge			26	AnAge	150	(56)	74	(56)		
Arctic fox *(Vulpes lagopus)*	38.6	AnAge			5.2	AnAge						
Red fox *(Vulpes vulpes)*	38.7	AnAge			4.58	PanTHERIA						
Eurasian lynx *(Lynx lynx)*					19.3	PanTHERIA						
Least weasel *(Mustela nivalis)*					0.0469	AnAge						
Primates												
Human *(Homo sapiens)*	37	AnAge	3.35	(53)	70	AnAge	123	(56)	78	(56)	70	(50)

Abbreviation: BT, body temperature; BW, bodyweight; BP, blood pressure; AnAge, The Animal Ageing and Longevity Database, PanTHERIA (http://esapubs.org/archive/ecol/e090/184/)

Table S4. Thyroid hormone levels in vertebrates.

Animal Species	Latin name	TT4 (nM)	Ref.	TT3 (nM)	Ref.	FT4 (pM)	Ref.	FT3 (pM)	Ref.
Pisces									
Zebrafish	*Danio rerio*	11.5	(60)						
Amphibia									
African clawed frog	*Xenopus laevis*	4.9	(61)	0.6	(61)				
Reptilia									
Western fence lizard	*Sceloporus occidentalis*	6.2	(62)						
Green anole	*Anolis carolinensis*	4.9	(63)						
Mammalia									
Monotremata									
Platypus	*Ornithorhynchus anatinus*	60.3	(11)	0.9	(11)				
Short-beaked echidna	*Tachyglossus aculeatus*	15.2	(11)	1.6	(11)	20.3	(11)	4.5	(11)
Chiroptera									
Little brown bat	*Myotis lucifugus*	15.4	(64)						
Lagomorpha									
Rabbit	*Oryctolagus cuniculus*	22	(11)						
Rodentia									
Mouse	*Mus musculus*	50.5	(11)	1.3	(11)	14.1	(11)	7.6	(11)
Guinea pig	*Cavia porcellus*	39	(11)	0.6	(11)	17	(11)	4	(11)
Rat	*Rattus norvegicus*	43.8	(11)	0.9	(11)	16.7	(11)	1.7	(11)
Artiodactyla									
Calf	*Bos taurus*	49	(11)						
Swine	*Sus scrofa*	46	(11)						
Perissodactyla									
Domestic horse	*Equus caballus*	34.8	(11)	1.2	(11)	33.2	(11)	8.8	(11)
Primates									
Human	*Homo sapiens*	100	(11)	1.9	(11)	16.4	(11)	16.4	(11)

Abbreviation: TT4, total T4; TT3, total T3; FT4, free T4; FT3, free T3

Table S5. Dosage and preparation of chemical compounds for neonatal mouse administration.

Compound	Dose (uL/g bodyweight)	Concentration (mg/mL)	Solvent	Notes
NH3	10	0.22	10% hydroxy-beta-cyclodextrin in water	
Propranolol	10	4	2 mM citrate (pH = 3) in saline	
Cyclosporin A	10	3	10% EtOH; 90% peanut oil	
PPARi (cocktail)	20	0.25 (each)	10% hydroxy-beta-cyclodextrin in water	GW6471, GSK3787,T0070907
Mifepristone	10	1	10% hydroxy-beta-cyclodextrin in water	
Somavert	10	1	Saline	
Hydralazine	10	0.5	Saline	
Losartan	10	1	Saline	
Atropine	10	0.5	Saline	
Nifedipine	10	0.1	Saline	
PTU	N/A	0.15% PTU	Chow	Iodine deficient diet

References and Notes

1. M. Xin, E. N. Olson, R. Bassel-Duby, Mending broken hearts: Cardiac development as a basis for adult heart regeneration and repair. *Nat. Rev. Mol. Cell Biol.* **14**, 529–541 (2013). doi:10.1038/nrm3619 Medline

2. G. Matrone, C. S. Tucker, M. A. Denvir, Cardiomyocyte proliferation in zebrafish and mammals: Lessons for human disease. *Cell. Mol. Life Sci.* **74**, 1367–1378 (2017). doi:10.1007/s00018-016-2404-x Medline

3. M. Patterson, L. Barske, B. Van Handel, C. D. Rau, P. Gan, A. Sharma, S. Parikh, M. Denholtz, Y. Huang, Y. Yamaguchi, H. Shen, H. Allayee, J. G. Crump, T. I. Force, C.-L. Lien, T. Makita, A. J. Lusis, S. R. Kumar, H. M. Sucov, Frequency of mononuclear diploid cardiomyocytes underlies natural variation in heart regeneration. *Nat. Genet.* **49**, 1346–1353 (2017). doi:10.1038/ng.3929 Medline

4. J. M. González-Rosa, M. Sharpe, D. Field, M. H. Soonpaa, L. J. Field, C. E. Burns, C. G. Burns, Myocardial Polyploidization Creates a Barrier to Heart Regeneration in Zebrafish. *Dev. Cell* **44**, 433–446.e7 (2018). doi:10.1016/j.devcel.2018.01.021 Medline

5. K. D. Poss, L. G. Wilson, M. T. Keating, Heart regeneration in zebrafish. *Science* **298**, 2188–2190 (2002). doi:10.1126/science.1077857 Medline

6. P. P. Rumyantsev, *Growth and Hyperplasia of Cardiac Muscle Cells*, B. M. Carlson, Ed. (Harwood, 1991).

7. M. Kleiber, Body size and metabolism. *Hilgardia* **6**, 315–353 (1932). doi:10.3733/hilg.v06n11p315

8. A. M. Makarieva, V. G. Gorshkov, B.-L. Li, S. L. Chown, P. B. Reich, V. M. Gavrilov, Mean mass-specific metabolic rates are strikingly similar across life's major domains: Evidence for life's metabolic optimum. *Proc. Natl. Acad. Sci. U.S.A.* **105**, 16994–16999 (2008). doi:10.1073/pnas.0802148105 Medline

9. K. Schmidt-Nielsen, L. Bolis, C. R. Taylor, Eds., *Comparative Physiology: Primitive Mammals* (Cambridge Univ. Press, 1980).

10. J. F. Gillooly, J. H. Brown, G. B. West, V. M. Savage, E. L. Charnov, Effects of size and temperature on metabolic rate. *Science* **293**, 2248–2251 (2001). doi:10.1126/science.1061967 Medline

11. A. J. Hulbert, Thyroid hormones and their effects: A new perspective. *Biol. Rev. Camb. Philos. Soc.* **75**, 519–631 (2000). doi:10.1017/S146479310000556X Medline

12. A. G. Little, F. Seebacher, The evolution of endothermy is explained by thyroid hormone-mediated responses to cold in early vertebrates. *J. Exp. Biol.* **217**, 1642–1648 (2014). doi:10.1242/jeb.088880 Medline

13. S. Friedrichsen, S. Christ, H. Heuer, M. K. H. Schäfer, A. Mansouri, K. Bauer, T. J. Visser, Regulation of iodothyronine deiodinases in the Pax8$^{-/-}$ mouse model of congenital hypothyroidism. *Endocrinology* **144**, 777–784 (2003). doi:10.1210/en.2002-220715 Medline

14. N. N. Chattergoon, G. D. Giraud, K. L. Thornburg, Thyroid hormone inhibits proliferation of fetal cardiac myocytes in vitro. *J. Endocrinol.* **192**, R1–R8 (2007). doi:10.1677/JOE-06-0114 Medline

15. X. Yang, M. Rodriguez, L. Pabon, K. A. Fischer, H. Reinecke, M. Regnier, N. J. Sniadecki, H. Ruohola-Baker, C. E. Murry, Tri-iodo-l-thyronine promotes the maturation of human cardiomyocytes-derived from induced pluripotent stem cells. *J. Mol. Cell. Cardiol.* **72**, 296–304 (2014). doi:10.1016/j.yjmcc.2014.04.005 Medline

16. J. L. Segar, K. A. Volk, M. H. Lipman, T. D. Scholz, Thyroid hormone is required for growth adaptation to pressure load in the ovine fetal heart. *Exp. Physiol.* **98**, 722–733 (2013). doi:10.1113/expphysiol.2012.069435 Medline

17. A. C. Svensson Holm, I. Lindgren, H. Osterman, J. Altimiras, Thyroid hormone does not induce maturation of embryonic chicken cardiomyocytes in vitro. *Physiol. Rep.* **2**, e12182 (2014). doi:10.14814/phy2.12182 Medline

18. N. Naqvi, M. Li, J. W. Calvert, T. Tejada, J. P. Lambert, J. Wu, S. H. Kesteven, S. R. Holman, T. Matsuda, J. D. Lovelock, W. W. Howard, S. E. Iismaa, A. Y. Chan, B. H. Crawford, M. B. Wagner, D. I. K. Martin, D. J. Lefer, R. M. Graham, A. Husain, A proliferative burst during preadolescence establishes the final cardiomyocyte number. *Cell* **157**, 795–807 (2014). doi:10.1016/j.cell.2014.03.035 Medline

19. M. H. Soonpaa, D. C. Zebrowski, C. Platt, A. Rosenzweig, F. B. Engel, L. J. Field, Cardiomyocyte Cell-Cycle Activity during Preadolescence. *Cell* **163**, 781–782 (2015). doi:10.1016/j.cell.2015.10.037 Medline

20. K. Alkass, J. Panula, M. Westman, T.-D. Wu, J.-L. Guerquin-Kern, O. Bergmann, No Evidence for Cardiomyocyte Number Expansion in Preadolescent Mice. *Cell* **163**, 1026–1036 (2015). doi:10.1016/j.cell.2015.10.035 Medline

21. N. H. Nguyen, J. W. Apriletti, S. T. Cunha Lima, P. Webb, J. D. Baxter, T. S. Scanlan, Rational design and synthesis of a novel thyroid hormone antagonist that blocks coactivator recruitment. *J. Med. Chem.* **45**, 3310–3320 (2002). doi:10.1021/jm0201013 Medline

22. L. Quignodon, S. Vincent, H. Winter, J. Samarut, F. Flamant, A point mutation in the activation function 2 domain of thyroid hormone receptor α1 expressed after CRE-mediated recombination partially recapitulates hypothyroidism. *Mol. Endocrinol.* **21**, 2350–2360 (2007). doi:10.1210/me.2007-0176 Medline

23. S. M. Ceccarelli, O. Chomienne, M. Gubler, A. Arduini, Carnitine palmitoyltransferase (CPT) modulators: A medicinal chemistry perspective on 35 years of research. *J. Med. Chem.* **54**, 3109–3152 (2011). doi:10.1021/jm100809g Medline

24. A. S. Pereyra, L. Y. Hasek, K. L. Harris, A. G. Berman, F. W. Damen, C. J. Goergen, J. M. Ellis, Loss of cardiac carnitine palmitoyltransferase 2 results in rapamycin-resistant, acetylation-independent hypertrophy. *J. Biol. Chem.* **292**, 18443–18456 (2017). doi:10.1074/jbc.M117.800839 Medline

25. B. N. Puente, W. Kimura, S. A. Muralidhar, J. Moon, J. F. Amatruda, K. L. Phelps, D. Grinsfelder, B. A. Rothermel, R. Chen, J. A. Garcia, C. X. Santos, S. Thet, E. Mori, M. T. Kinter, P. M. Rindler, S. Zacchigna, S. Mukherjee, D. J. Chen, A. I. Mahmoud, M.

Giacca, P. S. Rabinovitch, A. Aroumougame, A. M. Shah, L. I. Szweda, H. A. Sadek, The oxygen-rich postnatal environment induces cardiomyocyte cell-cycle arrest through DNA damage response. *Cell* **157**, 565–579 (2014). doi:10.1016/j.cell.2014.03.032 Medline

26. G. Tao, P. C. Kahr, Y. Morikawa, M. Zhang, M. Rahmani, T. R. Heallen, L. Li, Z. Sun, E. N. Olson, B. A. Amendt, J. F. Martin, Pitx2 promotes heart repair by activating the antioxidant response after cardiac injury. *Nature* **534**, 119–123 (2016). doi:10.1038/nature17959 Medline

27. K. Lagerspetz, Postnatal development of thermoregulation in laboratory mice. *Helgol. Wiss. Meeresunters.* **14**, 559–571 (1966). doi:10.1007/BF01611645

28. K. Gauthier, M. Plateroti, C. B. Harvey, G. R. Williams, R. E. Weiss, S. Refetoff, J. F. Willott, V. Sundin, J.-P. Roux, L. Malaval, M. Hara, J. Samarut, O. Chassande, Genetic analysis reveals different functions for the products of the thyroid hormone receptor alpha locus. *Mol. Cell. Biol.* **21**, 4748–4760 (2001). doi:10.1128/MCB.21.14.4748-4760.2001 Medline

29. R. Agah, P. A. Frenkel, B. A. French, L. H. Michael, P. A. Overbeek, M. D. Schneider, Gene recombination in postmitotic cells. Targeted expression of Cre recombinase provokes cardiac-restricted, site-specific rearrangement in adult ventricular muscle in vivo. *J. Clin. Invest.* **100**, 169–179 (1997). doi:10.1172/JCI119509 Medline

30. M. Lewandoski, E. N. Meyers, G. R. Martin, Analysis of Fgf8 gene function in vertebrate development. *Cold Spring Harb. Symp. Quant. Biol.* **62**, 159–168 (1997). doi:10.1101/SQB.1997.062.01.021 Medline

31. D. S. Sohal, M. Nghiem, M. A. Crackower, S. A. Witt, T. R. Kimball, K. M. Tymitz, J. M. Penninger, J. D. Molkentin, Temporally regulated and tissue-specific gene manipulations in the adult and embryonic heart using a tamoxifen-inducible Cre protein. *Circ. Res.* **89**, 20–25 (2001). doi:10.1161/hh1301.092687 Medline

32. J. Lee, J. M. Ellis, M. J. Wolfgang, Adipose fatty acid oxidation is required for thermogenesis and potentiates oxidative stress-induced inflammation. *Cell Reports* **10**, 266–279 (2015). 10.1016/j.celrep.2014.12.023 Medline

33. M. R. E. Symonds, S. P. Blomberg, in *Modern Phylogenetic Comparative Methods and Their Application in Evolutionary Biology*, L. Garamszegi, Ed. (Springer, Berlin, Heidelberg, 2014).

34. I. Rebrin, S. Kamzalov, R. S. Sohal, Effects of age and caloric restriction on glutathione redox state in mice. *Free Radic. Biol. Med.* **35**, 626–635 (2003). doi:10.1016/S0891-5849(03)00388-5 Medline

35. G. N. Huang, J. E. Thatcher, J. McAnally, Y. Kong, X. Qi, W. Tan, J. M. DiMaio, J. F. Amatruda, R. D. Gerard, J. A. Hill, R. Bassel-Duby, E. N. Olson, C/EBP transcription factors mediate epicardial activation during heart development and injury. *Science* **338**, 1599–1603 (2012). doi:10.1126/science.1229765 Medline

36. K. Hirose, N. Shimoda, Y. Kikuchi, Transient reduction of 5-methylcytosine and 5-hydroxymethylcytosine is associated with active DNA demethylation during regeneration of zebrafish fin. *Epigenetics* **8**, 899–906 (2013). doi:10.4161/epi.25653 Medline

37. T. C. Dembinski, C. K. H. Leung, R. P. C. Shiu, Evidence for a novel pituitary factor that potentiates the mitogenic effect of estrogen in human breast cancer cells. *Cancer Res.* **45**, 3083–3089 (1985). Medline

38. J. O. Oberpriller, J. C. Oberpriller, A. M. Arefyeva, V. I. Mitashov, B. M. Carlson, Nuclear characteristics of cardiac myocytes following the proliferative response to mincing of the myocardium in the adult newt, Notophthalmus viridescens. *Cell Tissue Res.* **253**, 619–624 (1988). doi:10.1007/BF00219752 Medline

39. O. V. Anatskaya, A. E. Vinogradov, Paradoxical relationship between protein content and nucleolar activity in mammalian cardiomyocytes. *Genome* **47**, 565–578 (2004). doi:10.1139/g04-015 Medline

40. W. R. Barrionuevo, W. W. Burggren, O_2 consumption and heart rate in developing zebrafish (Danio rerio): Influence of temperature and ambient O_2. *Am. J. Physiol.* **276**, R505–R513 (1999). Medline

41. S. Jiang, D. L. Claussen, The resting and active metabolism of red-spotted newts (Notophthalmus viridescens) on land at simulated winter and summer temperatures. *Comp. Biochem. Physiol. Part A. Physiol.* **104**, 805–811 (1993). doi:10.1016/0300-9629(93)90158-Z

42. C. Carey, Aerobic and anaerobic energy expenditure during rest and activity in montane Bufo b. boreas and Rana pipiens. *Oecologia* **39**, 213–228 (1979). doi:10.1007/BF00348070 Medline

43. H. L. Bartlett, R. B. Escalera 2nd, S. S. Patel, E. W. Wedemeyer, K. A. Volk, J. L. Lohr, B. E. Reinking, Echocardiographic assessment of cardiac morphology and function in Xenopus. *Comp. Med.* **60**, 107–113 (2010). Medline

44. J. S. Tsuji, Seasonal Profiles of Standard Metabolic Rate of Lizards (Sceloporus occidentalis) in Relation to Latitude. *Physiol. Zool.* **61**, 230–240 (1988). doi:10.1086/physzool.61.3.30161236

45. C. Francis, G. R. Brooks, Oxygen consumption, rate of heart beat and ventilatory rate in parietalectomized lizards, Sceloporus occidentalis. *Comp. Biochem. Physiol.* **35**, 463–469 (1970). doi:10.1016/0010-406X(70)90609-2

46. K. S. Orrell, J. D. Congdon, T. A. Jenssen, R. H. Michener, T. H. Kunz, Intersexual differences in energy expenditure of Anolis carolinensis lizards during breeding and postbreeding seasons. *Physiol. Biochem. Zool.* **77**, 50–64 (2004). doi:10.1086/383497 Medline

47. T. R. Grant, T. Dawson, Temperature Regulation in the Platypus, Ornithorhynchus anatinus: Production and Loss of Metabolic Heat in Air and Water. *Physiol. Zool.* **51**, 315–332 (1978). doi:10.1086/physzool.51.4.30160956

48. S. L. Deem, *Fowler's Zoo and Wild Animal Medicine, Volume 8* (2015); http://www.sciencedirect.com/science/article/pii/B9781455773978000736).

49. H. S. T. de Oliveira, *Ritmo Biologico Da Temperatura Corporal Em Preguicas* (Universidade Federal de Pernambuco, 2007).

50. R. S. Seymour, A. J. Blaylock, The principle of laplace and scaling of ventricular wall stress and blood pressure in mammals and birds. *Physiol. Biochem. Zool.* **73**, 389–405 (2000). doi:10.1086/317741 Medline

51. G. Neuweiler, *The Biology of Bats* (Oxford Univ. Press, 2000).

52. B. K. McNab, Complications inherent in scaling the basal rate of metabolism in mammals. *Q. Rev. Biol.* **63**, 25–54 (1988). doi:10.1086/415715 Medline

53. M. A. Holliday, D. Potter, A. Jarrah, S. Bearg, The relation of metabolic rate to body weight and organ size. *Pediatr. Res.* **1**, 185–195 (1967). doi:10.1203/00006450-196705000-00005 Medline

54. T. Dawson, Allometric Relations and Scaling Laws for the Cardiovascular System of Mammals. *Systems* **2**, 168–185 (2014). doi:10.3390/systems2020168

55. B. K. McNab, P. Morrison, Body temperature and metabolism in subspecies of Peromyscus from arid and mesic. *Ecol. Monogr.* **33**, 63–82 (1963). doi:10.2307/1948477

56. C. R. White, R. S. Seymour, The role of gravity in the evolution of mammalian blood pressure. *Evolution* **68**, 901–908 (2014). Medline

57. D. T. Beatty, A. Barnes, E. Taylor, D. Pethick, M. McCarthy, S. K. Maloney, Physiological responses of Bos taurus and Bos indicus cattle to prolonged, continuous heat and humidity. *J. Anim. Sci.* **84**, 972–985 (2006). doi:10.2527/2006.844972x Medline

58. I. Blei, G. Odian, *General, Organic, and Biochemistry: Connecting Chemistry to Your Life* (W. H. Freeman, 2005).

59. J. C. George, thesis, The University of Alaska Fairbanks. (2009).

60. L. T. M. van der Ven, E. J. van den Brandhof, J. H. Vos, D. M. Power, P. W. Wester, Effects of the antithyroid agent propylthiouracil in a partial life cycle assay with zebrafish. *Environ. Sci. Technol.* **40**, 74–81 (2006). doi:10.1021/es050972c Medline

61. M. Leloup, J. Buscaglia, Triiodothyronine, hormone of amphibian metamorphosis. *Acad. Sci. Czech Republic.* **284**, 2261–2263 (1977).

62. H. B. John-Alder, Thyroid regulation of resting metabolic rate and intermediary metabolic enzymes in a lizard (Sceloporus occidentalis). *Gen. Comp. Endocrinol.* **77**, 52–62 (1990). doi:10.1016/0016-6480(90)90205-Z Medline

63. P. Licht, R. J. Denver, Effects of TRH on hormone release from pituitaries of the lizard, Anolis carolinensis. *Gen. Comp. Endocrinol.* **70**, 355–362 (1988). doi:10.1016/0016-6480(88)90109-8 Medline

64. D. A. Damassa, A. W. Gustafson, G. G. Kwiecinski, G. A. Gagin, Seasonal influences on the control of plasma sex hormone-binding globulin by T4 in male little brown bats. *Am. J. Physiol.* **268**, R1303–R1309 (1995). Medline

65. J. O. Oberpriller, J. C. Oberpriller, Response of the adult newt ventricle to injury. *J. Exp. Zool.* **187**, 249–253 (1974). doi:10.1002/jez.1401870208 Medline